(22) M. L. H. Green, L. Pratt, and G. Wilkinson, *J. Chem. Soc.*, 3753 (1959).
(23) A. N. Nesmeyanov, I. I. Kritskaya, Yu. A. Ustinyuk, and E. I. Fedin, *Dokl. Akad. Nauk SSSR*, **176**, 341 (1968).
(24) F. A. Cotton and J. M. Troup, *J. Am. Chem. Soc.*, **96**, 3438 (1974).
(25) D. J. Darensbourg, H. H. Nelson, III, and C. L. Hyde, *Inorg. Chem.*, **13**, 2135 (1974).
(26) G. W. Griffin and L. I. Peterson, *J. Am. Chem. Soc.*, **65**, 2268 (1963).
(27) R. B. King, *J. Am. Chem. Soc.*, **91**, 7217 (1969).
(28) H. W. Whitlock, Jr., C. Reich, and W. D. Woessner, *J. Am. Chem. Soc.*, **93**, 2483 (1971).

Axial Ligation Modes in Iron(III) Porphyrins. Models for the Oxidized Reaction States of Cytochrome P-450 Enzymes and the Molecular Structure of Iron(III) Protoporphyrin IX Dimethyl Ester *p*-Nitrobenzenethiolate

S. C. Tang,[1a] S. Koch,[1a] G. C. Papaefthymiou,[1b] S. Foner,[1b] R. B. Frankel,*[1b] James A. Ibers,*[1c] and R. H. Holm*[1a,d]

Contribution from the Department of Chemistry and the Francis Bitter National Magnet Laboratory, Massachusetts Institute of Technology, Cambridge, Massachusetts 02139, and the Department of Chemistry, Northwestern University, Evanston, Illinois 60201.
Received July 17, 1975

Abstract: Cytochrome P-450 monooxygenase enzymes contain a protoporphyrin IX prosthetic group and exhibit five reaction states, in each of which the nature of axial ligation to Fe(II, III) is uncertain. The occurrence of sulfur coordination has been a matter of active speculation. The two oxidized states, ox-P-450 (resting, low spin) and ox-P-450·S (substrate bound, high spin), contain Fe(III) with apparent six and five coordination, respectively. In an attempt to develop experimental criteria for identifying axial ligands in iron(III) porphyrins, the series of complexes Fe(P)L (high spin) and Fe(P)LL′ (low spin), P = octaethylporphyrin, protoporphyrin IX dimethyl ester (PPIXDME) dianions, have been isolated and generated in situ, respectively, and subjected to detailed physical studies. Axial ligands L and L′ include a variety of oxygen, sulfur, and nitrogen donors intended to model possible protein side chain coordination. Isolable Fe(P)SR complexes were obtained with R = aryl. The crystal structure of Fe(PPIXDME)(SC_6H_4-*p*-NO_2) has been determined by x-ray diffraction techniques utilizing 6320 observations collected by counter methods. The compound crystallizes in space group C_i^1-$P\bar{1}$ with two molecules in a cell of dimensions a = 13.585 (6), b = 14.016 (2), c = 13.297 (2) Å, α = 110.83 (2), β = 119.74 (2), and γ = 62.60 (2)°. The observed density of 1.35 (2) g cm^{-3} compares favorably with the calculated density of 1.378 g cm^{-3}. Refinement of an anisotropic model (497 variables) by full-matrix least-squares methods leads to a conventional R index (on F^2) of 0.126 for the 6320 observations and to a conventional R index (on F) of 0.071 for the 3225 observations having $F_o > 3\sigma(F_o)$. The molecule exhibits near square pyramidal geometry with an Fe–S distance of 2.324 (2) Å and Fe–N distances ranging from 2.042 (5) to 2.081 (5) and averaging to 2.064 Å. The iron atom is 0.448 Å above the mean plane of the porphyrin core, which is nearly planar (mean deviation from the mean plane is 0.038 Å) but exhibits a slight ruffling that corresponds roughly to an S_4 distortion. Although the mean dimensions within the porphyrin agree well with previously reported values, there is a perceptible alternation in the lengths of the C_b–C_a bonds around the periphery of the porphyrin as well as an alternation of the C_a–C_m bonds such that there occurs a long-short-long-short . . . sequence of C_b–C_a, C_a–C_m, C_m–C_a, C_a–C_b bonds. The phenyl ring makes a dihedral angle of 11.1° with the porphyrin plane, and is situated away from the bulky propionic ester substituents. Extensive compilations of results are presented and include (i) electronic spectral data, (ii) principal g values evaluated from EPR spectra, (iii) Mössbauer parameters, (iv) effective magnetic moment values and crystal field parameters obtained from field dependent (≤60 kOe) magnetization data. Of the species Fe(P)L (L = ArS^-, ArO^-, OAc^-) and acidmetmyoglobin or hemoglobin, Fe(PPIXDME)(SAr) complexes provide the closest approach to the optical, EPR, and Mössbauer properties of ox-P-450·S. Of interest are the values of the saturation magnetic hyperfine field at the Fe nucleus, obtained from high-field (≤80 kOe) Mössbauer and magnetization measurements at 4.2 K. For L = O- and N-donor ligands $H_{hf}^0 \gtrsim -500$ kOe whereas $H_{hf}^0 = -476 \pm 10$ and -448 ± 10 kOe for Fe(PPIXDME)(SC_6H_4-*p*-NO_2) and ox-P-450_{cam}·S, respectively. Low-temperature optical and EPR spectra of Fe(P)LL′ complexes (L = N-, O-, S-donor ligands) together with data for cytochromes *b* and *c*, when compared with corresponding enzyme properties, indicate thiolate sulfur coordination in ox-P-450. With the provisos that not all possible axial ligation modes of the enzyme, simulated by L or L/L′ combinations, could be experimentally tested and that synthetic porphyrins may have limitations as models of biological heme coordination the following conclusions are drawn: (i) the most probable axial ligation mode in the ox-P-450·S state is Cys-S-Fe; (ii) the most probable modes in the ox-P-450 state are Cys-S-Fe-L′, with L′ = His, Lys(Arg), Cys-SH, Met, and Asn(Gln). No further conclusions regarding L could be drawn from the experimental data obtained here.

The cytochrome P-450 enzymes are prominent members of the monoxygenase (mixed-function oxidase) class of enzymes which catalyze the incorporation of one atom of dioxygen into a substrate while the other is reduced to water. The P-450 enzymes, also designated as cytochromes *m* in a recent nomenclature proposal,[2] are found in mammalian microsomes and mitochondria, and in bacteria. They have been implicated in the mammalian metabolism of lipids and steroids, amino acid biosynthesis, oxidative degradation of numerous xenobiotics, and facilitate yeast and bacterial growth on nonphysiological carbon sources. The biological and physical properties of these enzymes have been summarized or reviewed elsewhere.[3-9]

A significant advance in clarifying the nature of P-450-dependent oxygenase reactions has been the isolation, purification, and crystallization of the cytochrome P-450 en-

zyme from *Pseudomonas putida* grown on camphor.[10-12] It as well as the components of the coupled electron transfer chain, a reductase and the 2Fe-2S protein putidaredoxin, are soluble, permitting in vitro assembly of the enzyme system and deduction of the reaction sequence 1.[8,11] Here S is

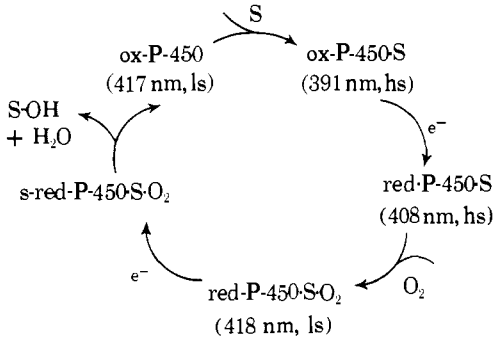

(1)

substrate, S-OH is hydroxylated product, ox = Fe(III), red = Fe(II), and s-red represents the unit with oxidation level $Fe^{II}\cdot O_2^-$; the electron transfer chain is not of direct relevance here and is omitted. The sequence contains five distinct reaction states of the cytochrome, of which all but the short-lived s-red form have been isolated or generated and examined separately. The remaining four reaction states each have distinctive physical properties including the different Soret band maxima indicated. Ample evidence exists (vide infra) to show that the oxidized states contain Fe(III) mainly in a high-spin (hs, $S = 5/2$) or low-spin (ls, $S = 1/2$) configuration, and the reduced states contain high- ($S = 2$) or low-spin ($S = 0$) Fe(II).[4a,7a,8] More recently, membrane-bound microsomal P-450 enzymes have been purified to apparent homogeneity and enzyme systems assembled.[13] While recent findings for one microsomal system[14] suggest a reactivity cycle different in several respects from scheme 1, the collective evidence for bacterial, microsomal, and mitochondrial enzymes indicates the existence of reaction states corresponding to the stable Fe(II, III) states in this scheme. Carbonylation of the reduced forms of these enzymes yields heme-CO complexes with a Soret band near 450 nm, from which this group of enzymes derives its P-450 designation.

While elucidation of the foregoing reaction sequence had led to a unified view of the component steps and overall course of action in the $P\text{-}450_{cam}$[15] enzyme system, the matter of precise chemical definition of each reaction state in this and other systems remains open in the absence of x-ray structural information. The nature of the prosthetic group is not in question, having been identified as an iron PPIX unit in $P\text{-}450_{cam}$[10,16] and a liver microsomal[17] cytochrome. However, for no reaction state is the identity of the axial ligands definitely established. The amino acid composition is known for the *P. putida*[8,18a] and a liver microsomal[18b] cytochrome, and reveals the presence of all residues with known or potential ligating groups (CH_2SH, CH_2SMe, COOH, C_6H_4OH, $CONH_2$, CH_2OH, Im, CH_2NH_2) in metalloproteins.[19] Included among these residues in the bacterial cytochrome are 6 Cys, 9 Met, 9 Tyr, 12 His, and 42 Glu (the most numerous residue).

The position of the Soret maximum of various red-P-450·CO species at ~450 nm, as opposed to ca. 410–420 nm in numerous other heme-CO pigments, has led to the frequent supposition that at least in the reduced cytochromes an "unconventional" axial ligand is present. Noting that microsomal P-450 cytochromes were inactivated by sulfhydryl reagents, Mason et al.[20] first proposed axial sulfur coordination. This proposal was strengthened by the finding that thiol addition to acid-met Mb and Hb afforded EPR g values close to those for low-spin cytochromes P-450.[21,22] Also, the addition of various thiols (including cysteine) to Fe(PPIX)Cl in the presence of nitrogenous bases gives similar results, viz., low-spin rhombic spectra with g values near 2.4, 2.2, and 1.9.[22,23] In the intervening period other lines of evidence, some of which are referred to in subsequent sections, have been brought to bear on the problem of axial ligand identification.

The possibility of axial sulfur ligation[3,7b,8] to the protoheme in one or more of the P-450 reaction states has proven difficult to evaluate critically in the absence of known properties of fully characterized sulfur-bound iron porphyrins. Indeed, prior to the inception of this and related studies on synthetic tetraaza (non-porphyrin) macrocyclic iron complexes,[24] the basic tetragonal $[FeN_4(SR)]$ coordination unit was unknown in stable isolable complexes. Inasmuch as the structural, electronic, and reactivity properties of both natural and synthetic iron(II, III) porphyrin complexes are significantly dependent upon the interaction of heme-iron with its axial ligand(s), we have attempted to develop in this investigation certain empirical criteria for the identity of ligands L and L′ in porphyrin complexes containing the high-spin $[Fe^{III}N_4L]$ and low-spin $[Fe^{III}N_4LL']$ coordination units (L,L′ = O-, S-, N-donor ligands). The basic assumption in this approach is that, at nominal parity of axial ligand(s), properties of the synthetic porphyrins and enzyme active sites will be sufficiently similar to allow deduction of axial ligation modes in the latter. The principal concern here is with characterization of the *Fe(III)* reaction states ox-P-450 (resting state) and ox-P-450·S (substrate-bound state). This account amplifies and extends our previous brief report[25] and describes the synthesis and properties of ferric porphyrin thiolates, including full structural details for $Fe(PPIXDME)(SC_6H_4\text{-}p\text{-}NO_2)$. Other than the work on related Fe(TPP)(SR) complexes,[26] which is contemporaneous with our own, the only report of complexes of this type prior to our original communication[25] is the presentation of an electronic spectrum of iron(III) deuteroporphyrin IX dimethyl ester benzenethiolate.[27] Very recently, however, Ogoshi et al.[28] have prepared a series of Fe(OEP)(SR) complexes as possible P-450 models.

Experimental Section

Preparation of Compounds. *p*-Nitrobenzenethiol (technical grade, Eastern Chemical Co.) was treated with aqueous sodium hydroxide in boiling ethanol, the hot solution filtered, and the filtrate acidified with HCl. The crude product was recrystallized from 2-propanol to yield yellow crystals, mp 75–77 °C. *p*-Nitrophenol (Eastman) was purified by recrystallization from toluene. Hemin chloride (three times recrystallized) was obtained from Nutritional Biochemicals Corp. Toluene and dichloromethane were dried over CaH_2 and P_2O_5, respectively; 2-methyltetrahydrofuran and methylcyclohexane were distilled from sodium benzophenone ketyl prior to use. All other chemicals were of reagent grade quality. Melting points were determined in evacuated capillaries and are uncorrected.

Iron(III) Protoporphyrin IX Dimethyl Ester Complexes. Fe(PPIXDME)Cl[29] and $[Fe(PPIXDME)]_2O$[30] were obtained by published methods. Preparations of thiolate and phenolate complexes were conducted under a pure dinitrogen atmosphere.

(a) Fe(PPIXDME)(SC_6H_4-*p*-NO_2). To a solution of 0.40 g (0.31 mmol) of $[Fe(PPIXDME)]_2O$ in 20 ml of toluene was added 0.19 g (1.2 mmol) of *p*-nitrobenzenethiol in 5 ml of toluene at room temperature. The reaction mixture was stirred for 15 min during which time the solution changed from brown-green to brown. Cooling to −20 °C afforded a crystalline product (0.44 g, 90%) which was collected by filtration and washed with a small amount of toluene, mp 162–163 °C. Anal. Calcd for $C_{42}H_{40}N_5O_6SFe$: C, 63.16; H, 5.05; N, 8.77; S, 4.01; Fe, 6.99. Found: C, 63.09; H, 5.15; N, 8.74; S, 4.15; Fe, 7.26.

(b) Fe(PPIXDME)(SC_6H_4-*p*-Cl). The preceding method was employed using *p*-chlorobenzenethiol (6 equiv) and a reaction time of

Table I. Summary of Crystal Data and Intensity Collection

Formula	$C_{42}H_{40}FeN_5O_6S$	
M	798.73 amu	
a, Å	13.585 (6)[a]	
b, Å	14.016 (2)	
c, Å	13.297 (2)	
α, deg	110.83 (2)	
β, deg	119.74 (2)	
γ, deg	62.60 (2)	
V, Å^3	1925	
Z	2	
d_{calcd}, g/cm^3	1.378	
d_{obsd}, g/cm^3	1.35 (2)	
Space group	C_i^1–$P\bar{1}$	
Crystal dimensions, nm	0.2 × 0.3 × 0.15	
Crystal volume, mm^3	0.009 44	
Receiving aperture	5.5 by 6.0 mm 32 cm from crystal	
Unique data	6320 total	
Number having $F_o^2 > 3\sigma(F_o^2)$	3225	
Radiation	Mo $K\alpha_1$ (0.709 30 Å)	Cu $K\alpha_1$ (1.540 562 Å)
μ, cm^{-1}	4.94	40.82
Transmission factors	0.90–0.94	0.413–0.617
Takeoff angle, deg	2.8	3.2
Scan speed	2 deg in 2θ/min	1 deg in 2θ/min
Scan range	0.85 below $K\alpha_1$ to 0.75 above $K\alpha_2$	0.85 below $K\alpha_1$ to 0.85 above $K\alpha_2$
2θ range, deg	0 to 42.6	104.25 to 127
Background counts	10 s $2\theta \leq 33.5$, 20 s $33.5 < 2\theta \leq 38.0$, 40 s $38.0 < 2\theta \leq 42.6$	40 s
Data collected	$h \geq 0$	$h \leq 0$

[a] Cell constants were derived from measurements with Cu $K\alpha_1$ radiation. The reduced cell is derived from the present cell by the transformation matrix $(101, 0\bar{1}0, 00\bar{1})$ and has the dimensions a = 13.497, b = 14.016, c = 13.297 Å, α = 110.83, β = 119.07, γ = 96.48°.

45 min at room temperature. The product was isolated as blue-black crystals in 75% yield, mp 112–113 °C. Anal. Calcd for $C_{42}H_{40}ClN_4O_4SFe$: C, 63.99; H, 5.12; N, 7.11; S, 4.07; Fe, 7.09. Found: C, 63.67; H, 4.89; N, 7.09; S, 4.08; Fe, 6.94.

(c) **Fe(PPIXDME)(OC$_6$H$_4$-*p*-NO$_2$).** To a solution of 0.40 g (0.31 mmol) of $[Fe(PPIXDME)]_2O$ in 30 ml of toluene was added 0.26 g (1.9 mmol) of solid *p*-nitrophenol. Upon stirring for 30 min at room temperature the reaction mixture changed from brown-green to deep brown. The reaction mixture was then maintained at 65 °C for 3 h. Slow cooling afforded the product as a black microcrystalline product (0.45 g, 94%). Anal. Calcd for $C_{42}H_{40}N_5O_7Fe$: C, 64.45; H, 5.15; N, 8.95. Found: C, 64.69; H, 5.26; N, 8.88.

(d) **Fe(PPIXDME)(OEt).** To a warm solution of 0.20 g (0.15 mmol) of $[Fe(PPIXDME)]_2O$ in 3–4 ml of chloroform was added gradually 25 ml of hot ethanol. The solution was heated at 80 °C for 2 h and then allowed to cool slowly to −20 °C. The crystalline product was collected and once recrystallized from chloroform–ethanol to afford blue-black crystals which were washed with ethanol and dried in vacuo (0.20 g, 95%), mp 175–176 °C. Anal. Calcd for $C_{38}H_{41}N_4O_5Fe$: C, 66.18; H, 5.99; N, 8.12. Found: C, 65.95; H, 6.05; N, 7.94.

(e) **Fe(PPIXDME)(OAc).** A solution of $[Fe(PPIXDME)]_2O$ (0.20 g, 0.15 mmol) in a 30-ml mixture of 5:1 v/v glacial acetic acid–dichloromethane was maintained at reflux for 3 h. After cooling the reaction mixture to room temperature solvent was removed in vacuo and the solid residue was washed with 10 ml of cold 9:1 v/v toluene–glacial acetic acid, giving 0.15 g (70%) of blue-black product, mp 192–194 °C. Anal. Calcd for $C_{38}H_{39}N_4O_6Fe$: C, 64.87; H, 5.59; N, 7.96. Found: C, 64.97; H, 5.61; N, 8.10.

Iron(III) Octaethylporphyrin Complexes. Very pure octaethylporphyrin[31] was a gift from Professor H. H. Inhoffen. Fe(OEP)(OMe) and $[Fe(OEP)]_2O$ were obtained by the methods (or slight modifications thereof) described by Buchler and Schneehage.[32]

(a) **Fe(OEP)(SC$_6$H$_4$-*p*-NO$_2$).** *p*-Nitrobenzenethiol (0.40 g, 2.6 mmol) in 10 ml of toluene was added to a suspension of 0.60 g (0.50 mmol) of $[Fe(OEP)]_2O$ in 20 ml of toluene, and the reaction mixture was stirred for 1 h at room temperature. The product was collected from the cooled reaction mixture by filtration, washed with *n*-heptane, and dried in vacuo, affording dark purple crystals (0.65 g, 87%), mp 270 °C dec. Anal. Calcd for $C_{42}H_{48}N_5O_2SFe$: C, 67.92; H, 6.51; N, 9.43; S, 4.32. Found: C, 68.11; H, 6.66; N, 9.30; S, 4.13.

(b) **Fe(OEP)(SPh).** $[Fe(OEP)]_2O$ (0.20 g, 0.17 mmol) and diphenyl disulfide (0.40 g, 1.8 mmol) were suspended in 25 ml of toluene. On the addition of 0.25 ml (2.4 mmol) of benzenethiol all reactants dissolved, followed by crystallization of the product. This material was isolated and treated as in the preceding preparation, giving purple-black crystals (0.19 g, 81%), mp 220 °C dec. Anal. Calcd for $C_{42}H_{49}N_4SFe$: C, 72.29; H, 7.08; N, 8.03; S, 4.60. Found: C, 72.29; H, 7.11; N, 8.07; S, 4.50.

(c) **Fe(OEP)(OAc).** The following procedure was employed instead of that given earlier for this compound.[32] Octaethylporphyrin (1.0 g, 1.9 mmol) and basic ferric acetate[24b] (0.40 g, 2.1 mmol) were heated in glacial acetic acid for 2 h. The hot solution was filtered and the filtrate was allowed to stand at room temperature for 48 h. The product was collected by filtration, washed with ether, and air-dried, affording dark-purple crystals (0.90 g, 74%).

Physical Measurements. Owing to the sensitivity of the majority of complexes to dioxygen, all manipulations and measurements were performed under a pure dinitrogen atmosphere. Electronic spectra of solutions were recorded on a Cary Model 14 or 17 spectrophotometer. Spectra of complexes at 77 K in 2-methyltetrahydrofuran or toluene–methylcyclohexane glasses were obtained using the Model 17 instrument equipped with a quartz Dewar having a flat quartz cell of ca. 1-mm path length. EPR measurements were made with a Varian E-9 spectrometer operating at X-band frequencies. Sample temperatures were either 80–95 K or ~4.2 K with the latter obtained using the Varian E-245 liquid helium accessory. The magnetic field was monitored with a Harvey-Wells Precision NMR Gaussmeter (Model G-502) and the microwave frequency was measured with a Sperry microline frequency meter (Model 1241). A typical EPR sample consisted of 5–10 mg of complex, 0.4 ml of solvent, and ~10 equiv of added base. Magnetic susceptibilities were determined as previously described[24b] using a Bruker Faraday apparatus interfaced with a Leybold-Hereaus Helium flow-type cryostat operating at 20–295 K. Polarographic measurements were performed at 25.0 ± 0.1 °C with a PAR Model 170 Electrochemistry System using a rotating Pt working electrode, solutions ~10^{-3} M in complex and 0.05 M in (n-Bu$_4$N)(ClO$_4$) supporting electrolyte, and a saturated calomel reference electrode.

Mössbauer spectra were recorded on a multi-channel analyzer using a constant acceleration Mössbauer drive, calibrated with metallic iron absorbers. Spectra were taken at room temperature, 77 and 4.2 K, and in longitudinal magnetic fields up to 80 kOe at 4.2 K, using a Nb–Sn superconducting magnet. A 100 mCi ^{57}Co (in Rh matrix) source situated in zero field at the same temperature as the absorber and a Xe–CO_2 proportional counter provided counting rates up to 0.5 × 10^4 c/sec in the presence of solid absorbers. Absorber thicknesses of 3 to 5 mg of Fe/cm^2 were used, resulting on the average in 6 to 10% effects. Mössbauer parameters were obtained by fitting the Mössbauer spectra to Lorentzian lines except for cases of very broad line spectra that largely deviated from Lorentzian shapes.

Magnetization measurements at 4.2 K over a magnetic field range from zero to 55 kOe were obtained using a vibrating sample magnetometer adapted to a superconducting solenoid. Sample weights of the order of 20 to 50 mg were used in thin-walled Delrin (plastic) containers. Corrections for any paramagnetism of the empty containers and the diamagnetism of the samples were taken into account, but for the strongly paramagnetic samples studied these corrections were negligible.

Crystal Structure Determination. In an inert atmosphere box a suitable crystal of Fe(PPIXDME)(SC$_6$H$_4$-*p*-NO$_2$) was sealed in a soft-glass capillary. Preliminary photographs failed to reveal any symmetry other than a center of inversion. Intensity data were collected on a FACS-I diffractometer using Mo $K\alpha_1$ radiation initially. Because the structure appeared to be unusually well-behaved for a metalloporphyrin, the data set was extended using Cu $K\alpha_1$ radiation. Details regarding crystal parameters and collection of

Table II. Positional and Thermal Parameters for the Atoms of Fe(PPIXDME)(SC_6H_4-*p*-NO_2)

ATOM	X[A]	Y	Z	B11[B]	B22	B33	B12	B13	B23
FE	0.409547(84)	-0.070809(72)	0.086710(81)	9.56(10)	6.87(7)	8.89(9)	-2.13(7)	3.53(8)	2.16(6)
S	0.41103(17)	-0.22445(14)	0.11799(17)	13.92(21)	7.82(14)	14.00(20)	-2.29(13)	7.40(18)	3.35(13)
O(1)	0.21173(58)	0.35477(43)	0.42488(53)	18.00(80)	11.68(49)	17.24(74)	-3.68(53)	6.38(67)	1.51(47)
O(2)	0.33367(64)	0.42904(53)	0.44773(72)	26.5(11)	17.94(68)	36.5(13)	-8.13(70)	6.30(92)	13.65(78)
O(3)	-0.07846(47)	0.51516(40)	0.28171(44)	18.98(70)	8.91(42)	13.89(59)	-0.65(43)	7.68(52)	1.74(40)
O(4)	-0.12087(61)	0.39484(52)	0.31345(57)	28.8(10)	17.57(71)	21.21(83)	-8.34(68)	17.13(79)	-0.17(58)
O(5)	0.79373(67)	-0.59448(52)	-0.12197(66)	19.83(87)	15.00(69)	24.2(10)	-0.38(64)	12.60(87)	3.11(64)
O(6)	0.62594(76)	-0.59813(56)	-0.26810(69)	33.7(13)	19.92(79)	21.03(94)	-13.39(82)	17.22(99)	-7.79(70)
N(1)	0.35187(49)	-0.10134(38)	-0.09500(44)	12.44(62)	7.18(40)	9.04(50)	-2.90(40)	5.13(48)	1.79(36)
N(2)	0.57905(46)	-0.11413(38)	0.09606(47)	9.78(57)	6.70(40)	11.64(57)	-2.53(38)	5.13(49)	2.08(38)
N(3)	0.46376(47)	0.01732(38)	0.25471(43)	10.18(58)	7.17(39)	8.95(52)	-3.07(38)	2.62(46)	1.50(36)
N(4)	0.23523(42)	0.03154(37)	0.06419(43)	7.06(49)	7.28(39)	9.63(52)	-2.08(35)	2.84(43)	2.09(36)
N(5)	0.68273(88)	-0.56723(60)	-0.16794(85)	18.5(12)	9.57(67)	19.4(11)	-3.89(75)	10.3(11)	1.43(69)
C(1)	0.23286(64)	-0.08779(49)	-0.17254(60)	11.60(77)	7.31(49)	10.68(69)	-3.41(50)	4.25(63)	1.97(46)
C(2)	0.23036(75)	-0.14794(55)	-0.28785(60)	16.8(10)	9.49(58)	9.16(65)	-5.82(63)	5.61(71)	-0.09(48)
C(3)	0.34595(77)	-0.19286(55)	-0.27600(63)	18.8(10)	8.77(58)	9.99(69)	-4.99(63)	7.68(76)	0.49(50)
C(4)	0.42173(67)	-0.16459(49)	-0.15698(59)	13.40(83)	7.28(49)	9.79(65)	-3.04(52)	5.68(64)	1.73(45)
C(5)	0.54646(69)	-0.19629(50)	-0.10663(64)	14.44(87)	6.86(50)	12.96(75)	-2.66(53)	8.13(70)	1.43(49)
C(6)	0.62087(63)	-0.17427(50)	0.00865(65)	10.50(77)	7.52(51)	12.72(76)	-1.92(50)	4.99(66)	3.64(51)
C(7)	0.75070(65)	-0.21382(54)	0.05517(69)	12.04(80)	8.56(58)	15.00(83)	-2.44(54)	7.26(72)	3.22(57)
C(8)	0.78900(64)	-0.17493(55)	0.17223(75)	10.31(71)	9.39(59)	16.02(94)	-3.27(52)	5.64(72)	3.64(61)
C(9)	0.68428(59)	-0.11357(51)	0.19712(68)	7.27(68)	8.45(53)	13.68(81)	-2.17(47)	4.29(63)	3.12(53)
C(10)	0.68180(60)	-0.05841(54)	0.30623(62)	9.68(76)	10.02(59)	11.21(74)	-2.67(52)	2.58(64)	3.56(54)
C(11)	0.58286(58)	0.00070(49)	0.33340(59)	9.13(68)	8.43(53)	10.77(68)	-2.65(48)	3.90(59)	2.80(49)
C(12)	0.58459(65)	0.06052(53)	0.44912(57)	12.48(84)	9.27(57)	9.24(68)	-5.01(57)	2.60(65)	2.01(50)
C(13)	0.46827(61)	0.10813(51)	0.43838(58)	10.93(71)	8.30(54)	9.60(63)	-3.00(50)	3.42(58)	2.30(47)
C(14)	0.39416(59)	0.08102(49)	0.31810(57)	9.52(69)	7.76(49)	8.80(62)	-2.78(47)	3.36(56)	2.24(44)
C(15)	0.26904(62)	0.11712(49)	0.26766(57)	12.41(74)	7.18(50)	9.48(63)	-3.64(49)	5.16(58)	0.67(45)
C(16)	0.19474(59)	0.09715(48)	0.15310(62)	9.90(70)	6.42(48)	12.59(73)	-1.93(46)	5.72(62)	1.81(47)
C(17)	0.06377(59)	0.14211(50)	0.10158(63)	9.83(68)	7.47(52)	12.70(75)	-2.51(47)	5.08(62)	2.14(51)
C(18)	0.02570(58)	0.10268(48)	-0.01457(60)	9.31(67)	7.00(48)	12.05(71)	-2.34(45)	3.52(59)	2.82(47)
C(19)	0.13116(55)	0.03334(47)	-0.03750(57)	8.65(65)	6.79(46)	10.55(65)	-3.02(44)	2.26(54)	2.42(45)
C(20)	0.13333(61)	-0.02574(50)	-0.14631(57)	10.68(74)	7.92(50)	9.25(64)	-2.99(48)	1.97(58)	2.21(45)
C(21)	0.11071(82)	-0.15302(65)	-0.39665(58)	26.6(13)	13.86(85)	8.85(60)	-5.36(88)	5.44(74)	-0.22(55)
C(22)	0.3946(12)	-0.26409(80)	-0.36692(83)	28.8(17)	13.14(91)	13.15(97)	-9.2(10)	11.8(11)	-1.58(70)
C(23)	0.3775(19)	-0.3380(14)	-0.4272(13)	79.4(42)	32.5(25)	34.5(22)	-25.9(27)	36.0(27)	-7.8(17)
C(24)	0.82570(69)	-0.28760(60)	-0.01676(70)	17.53(96)	13.09(70)	20.0(10)	-5.20(65)	12.62(86)	1.78(66)
C(25)	0.91438(75)	-0.18844(81)	0.26210(96)	10.49(80)	15.5(11)	17.4(14)	-2.37(71)	6.33(94)	4.16(96)
C(26)	1.0098(13)	-0.2564(14)	0.2516(12)	23.7(23)	34.6(28)	31.4(19)	-0.9(20)	11.6(18)	12.8(19)
C(27)	0.69792(63)	0.06331(63)	0.55803(58)	13.82(81)	15.18(80)	10.76(67)	-6.89(67)	-0.45(59)	2.97(58)
C(28)	0.42745(69)	0.17657(55)	0.53581(59)	17.2(10)	10.07(58)	10.08(69)	-4.50(61)	6.23(71)	0.69(49)
C(29)	0.41937(70)	0.29536(57)	0.56054(65)	16.99(97)	9.60(58)	11.04(79)	-3.75(61)	5.66(73)	-0.01(55)
C(30)	0.31173(88)	0.36119(65)	0.47234(82)	17.5(11)	8.65(65)	15.7(11)	-4.93(76)	7.68(96)	-0.63(65)
C(31)	-0.01106(59)	0.21947(53)	0.16989(63)	9.83(76)	9.66(57)	14.78(83)	-1.25(51)	5.87(67)	2.90(54)
C(32)	-0.02381(66)	0.33693(53)	0.18128(64)	14.48(90)	9.08(52)	12.70(79)	-0.71(54)	6.71(73)	1.94(51)
C(33)	-0.07933(69)	0.41541(70)	0.26599(69)	11.88(85)	11.91(76)	12.09(81)	-2.53(64)	4.49(68)	3.23(64)
C(34)	-0.10175(55)	0.12805(55)	-0.10746(62)	7.81(60)	11.32(65)	14.84(79)	-2.52(49)	1.92(55)	4.30(58)
C(35)	0.48897(60)	-0.32688(49)	0.03399(59)	10.34(74)	7.86(51)	11.46(68)	-3.00(50)	4.74(61)	3.36(48)
C(36)	0.42877(62)	-0.37303(54)	-0.07888(66)	9.33(75)	8.20(55)	14.47(79)	-3.20(52)	3.55(65)	2.97(53)
C(37)	0.48912(71)	-0.45283(57)	-0.14649(67)	15.10(87)	8.77(58)	12.15(85)	-5.53(58)	3.76(73)	1.13(57)
C(38)	0.61589(73)	-0.48581(49)	-0.09529(72)	15.63(94)	5.55(46)	15.05(88)	-2.31(52)	8.71(80)	1.15(51)
C(39)	0.67777(62)	-0.44366(51)	0.01572(66)	11.51(80)	7.19(51)	13.56(77)	-1.49(51)	3.35(68)	3.85(51)
C(40)	0.61503(59)	-0.36595(51)	0.08097(61)	10.84(67)	7.31(49)	11.31(73)	-1.70(46)	3.14(60)	3.20(49)
ME(1)	0.2297(10)	0.50123(77)	0.3610(11)	38.2(18)	22.5(10)	49.7(22)	-5.9(11)	2.6(16)	26.9(13)
ME(2)	-0.11980(81)	0.59629(60)	0.37002(67)	26.5(13)	11.34(65)	12.49(81)	0.95(70)	8.06(88)	0.63(57)

[A] ESTIMATED STANDARD DEVIATIONS IN THE LEAST SIGNIFICANT FIGURE(S) ARE GIVEN IN PARENTHESES IN THIS AND ALL SUBSEQUENT TABLES. [B] THE FORM OF THE ANISOTROPIC THERMAL ELLIPSOID IS: $\exp(-(B11h^2 + B22k^2 + B33l^2 + 2B12hk + 2B13hl + 2B23kl))$. THE QUANTITIES GIVEN IN THE TABLE ARE THE THERMAL COEFFICIENTS $\times 10^3$.

intensity data are given in Table I. Details on computer programs, methods of processing, sources of atomic scattering factors and anomalous terms, and related items have been given previously[33] and will not be repeated here. The structure was solved from an origin-removed sharpened Patterson function. The correct solution was arrived at with some effort owing to the difficulty of distinguishing the Fe–Fe vector from a doubled Fe–S vector. The ensuing structure was refined by full-matrix least-squares methods. The final refinement, based on 497 variables (two scale factors and an anisotropic model for the 55 nonhydrogen atoms) and 6320 unique data, was carried out on the CDC 7600 computer facility at the Lawrence Berkeley Laboratories. In this refinement the quantity $\Sigma w(F_o^2 - F_c^2)^2$ was minimized, where the weight w is $1/\sigma^2(F_o^2)$ and the latter quantity was estimated from counting statistics and a p of 0.04. Included in the final refinement were fixed contributions from 36 of the 40 hydrogen atoms; the hydrogen atoms of the two β-carbon atoms of the vinyl groups could not be located on difference Fourier maps. The hydrogen atom positions were idealized, utilizing a C–H distance of 1.0 Å and an isotropic B value 1.0 Å^2 greater than for the carbon atom to which a given hydrogen atom is attached. The final R index on F^2 is 0.126 and the final weighted R index is 0.165. The error in an observation of unit weight is 1.7 e^2. The final R index on F for the 3225 observations having $F_o > 3\sigma(F_o)$ is 0.071. No final difference Fourier summation was computed, but a difference Fourier map on which the hydrogen atoms were located had a maximum density of 0.7 e/Å^3. An analysis of $\Sigma w(F_o^2 - F_c^2)^2$ as a function of F_o^2, Miller indices, and setting angles revealed no particular trends.

Table III. Idealized Positions of H Atoms

Atom	x	y	z	Atom	x	y	z
H(1)C(5)	0.589	−0.241	−0.160	H(2)C(29)	0.493	0.295	0.564
H(1)C(10)	0.760	−0.062	0.371	H(1)C(31)	−0.091	0.214	0.132
H(1)C(15)	0.228	0.164	0.321	H(2)C(31)	0.025	0.202	0.248
H(1)C(20)	0.055	−0.022	−0.212	H(1)C(32)	0.055	0.340	0.206
H(1)C(21)	0.041	−0.099	−0.380	H(2)C(32)	−0.073	0.360	0.105
H(2)C(21)	0.105	−0.137	−0.464	H(1)C(34)	−0.160	0.164	−0.073
H(3)C(21)	0.103	−0.222	−0.418	H(2)C(34)	−0.117	0.176	−0.155
H(1)C(22)	0.452	−0.239	−0.367	H(3)C(34)	−0.116	0.064	−0.159
H(1)C(24)	0.869	−0.359	0.004	H(1)C(36)	0.341	−0.348	−0.111
H(2)C(24)	0.773	−0.296	−0.100	H(1)C(37)	0.447	−0.486	−0.228
H(3)C(24)	0.881	−0.258	−0.006	H(1)C(39)	0.765	−0.467	0.048
H(1)C(25)	0.914	−0.134	0.335	H(1)C(40)	0.658	−0.336	0.162
H(1)C(27)	0.705	0.038	0.619	H(1)Me(1)	0.251	0.555	0.355
H(2)C(27)	0.769	0.022	0.542	H(2)Me(1)	0.211	0.456	0.278
H(3)C(27)	0.698	0.138	0.589	H(3)Me(1)	0.160	0.531	0.372
H(1)C(28)	0.348	0.177	0.514	H(1)Me(2)	−0.056	0.608	0.441
H(2)C(28)	0.481	0.144	0.605	H(2)Me(2)	−0.175	0.664	0.342
H(1)C(29)	0.418	0.330	0.637	H(3)Me(2)	−0.166	0.571	0.388

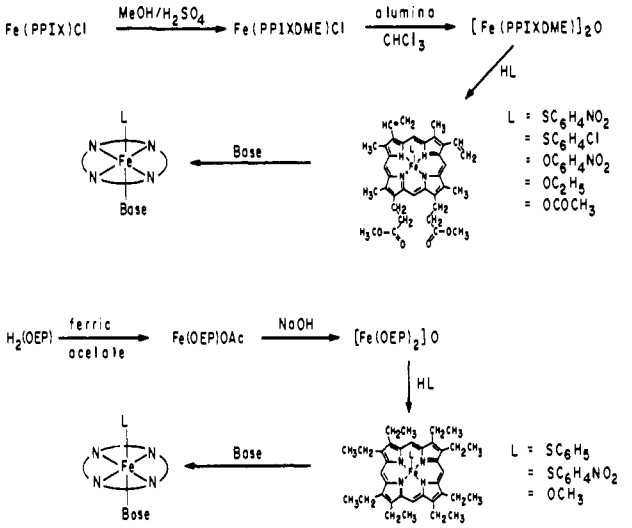

Figure 1. Synthetic scheme for the preparation of iron(III) PPIXDME and OEP complexes. The indicated five-coordinate complexes were isolated; six-coordinate base adducts were generated in situ and were not isolated.

The following data are tabulated: final positional and thermal parameters for the nonhydrogen atoms refined (Table II); idealized positions of the hydrogen atoms (Table III); root-mean-square amplitudes of vibration for the nonhydrogen atoms (Table IV[34]). A listing of F_o^2 vs. F_c^2 is available.[34]

Results and Discussion

The substrate binding reaction 2, which is the initial step in the enzyme reaction cycle 1, has been directly established for a number of P-450 cytochromes,[4,7,8,35] including P-450_{cam}, and results in the indicated spin-state change. In

$$\text{ox-P-450 (ls)} + \text{S} \rightleftarrows \text{ox-P-450·S (hs)} \qquad (2)$$

utilizing synthetic iron(III) porphyrin complexes for examination of axial ligation, an obvious first step is recognition of the following spin state–structure correlations: (i) high-spin complexes are five coordinate with the metal displaced from the porphyrin plane toward the axial ligand, and (ii) low-spin complexes are six coordinate with the iron nearly or exactly in the porphyrin mean plane. Spin states have been established by several techniques including magnetic susceptibility measurements.[36] Synthetic porphyrin,[37-39] Hb and Mb,[40,41a] and cytochrome *b* and *c*[41b] structures provide the basis of these correlations, for which there are no exceptions with synthetic complexes. Essentially the same statement applies to ferriheme proteins except that, as with acid-metMb,[40,41a] a more distantly bound sixth ligand may be present which, however, provides an insufficiently strong influence to alter the high-spin state. Consequently, the resting and substrate-bound forms are assigned effective six- and five-coordinate structures, respectively.

Synthesis of Compounds. Numerous five-coordinate iron(III) porphyrins Fe(P)L with L = halide, pseudohalide, RO^-, and RCO_2^- have been prepared.[27,29,30a,32] Of the complexes obtained in this study only the thiolates (L = RS^-) are of unusual synthetic interest. Because of the possibility that such complexes might be inherently unstable by virtue of the redox reaction 3, in which the initial event is presumably intramolecular reduction of Fe(III) by bound thiolate, both the porphyrins and the R substituent have

$$2\text{Fe}^{\text{III}}(\text{P})(\text{SR}) \rightarrow 2\text{Fe}^{\text{II}}\text{P} + \text{RSSR} \qquad (3)$$

been varied to provide a rough indication of the stability limits of Fe(P)(SR) species. Cathodic polarography in DMF solution indicates that the ease of reduction of Fe(III) to Fe(II) with a chloride axial ligand increases in the order Fe(TPP)Cl (−0.20) > Fe(PPIXDME)Cl (−0.31) > Fe(OEP)Cl (−0.39 V). The indicated $E_{1/2}$ values are similar to those reported for the same and related complexes.[42] Assuming the same order for thiolate complexes, preparation of these species was restricted to the OEP and PPIXDME cases. The preparation of thiolate and other five-coordinate iron(III) porphyrins is summarized in Figure 1. The μ-oxo dimers were chosen as precursors because they can be highly purified by chromatography, and their bridge cleavage products contained little, if any, magnetic impurities compared with those in the same products obtained by other methods. Stable compounds were obtained only with *aryl* thiolates; reaction of either the OEP or PPIXDME dimers with alkylthiols afforded no isolable Fe(III) product. While *p*-nitrobenzenethiolate complexes could be isolated with P = OEP and PPIXDME, a stable benzenethiolate complex was obtainable only in the OEP series. Fe(TPP)(SPh) is reported to decompose in benzene at 25 °C.[26] In a report which became available to us after this manuscript was submitted for publication Ogoshi et al.,[28] using a different method, have described the synthesis of several Fe(OEP)(SR) complexes with R = alkyl. These complexes are stated to be less stable than Fe(OEP)(SPh) in organic solvents. These results collectively indicate that relatively electronegative (less reducing) thiolates in combination with the porphyrins used here tend to afford the most stable complexes. Reaction of alkylthiolates with

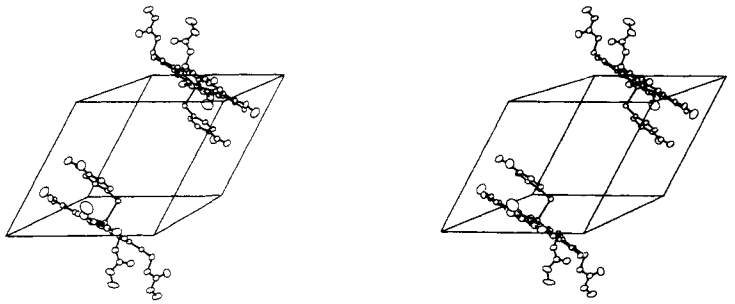

Figure 2. A stereoview of the unit cell of Fe(PPIXDME)($SC_6H_4NO_2$). The x axis is from left to right, the y axis is from bottom to top, and the z axis comes out of the page. Hydrogen atoms have been omitted for the sake of clarity. Atoms are drawn at their 20% probability ellipsoids.

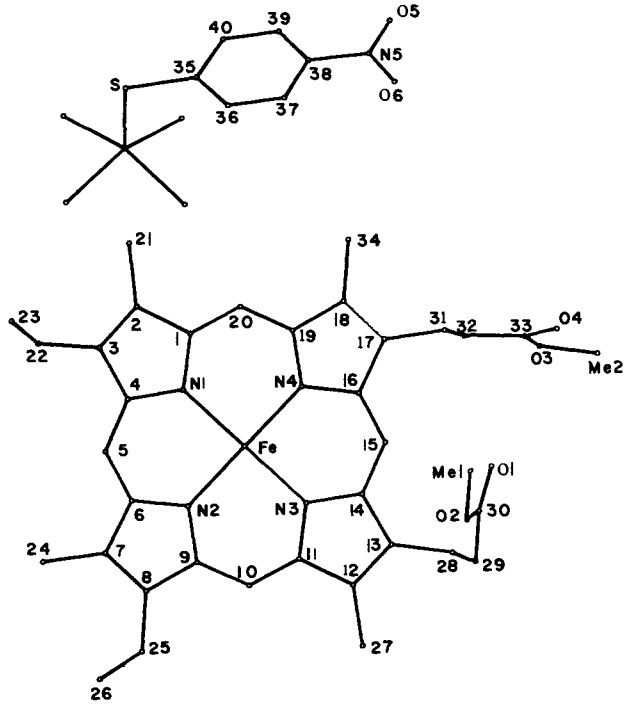

Figure 3. The numbering scheme for Fe(PPIXDME)($SC_6H_4NO_2$).

Table V. Axial Ligation Modes Examined in High- and Low-Spin Iron(III) Porphyrins Fe(P)L and Fe(P)LL' Based on Isolated Five-Coordinate PPIXDME and OEP Complexes

	Ligands L, L'	
Axial ligation	Potential biological	Synthetic
	High-Spin	
S^-–Fe	Cys	$O_2NC_6H_4S^-$, $ClC_6H_4S^-$, PhS^- (ArS^-)
O^-–Fe	Tyr	$O_2NC_6H_4O^-$, PhO^- (ArO^-)
	Asp, Glu	OAc^-
	Ser, Thr	OEt^-, OMe^- (RO^-)
N–Fe	His	[Acid-metMb, -Hb][b]
S–Fe	His, Lys, Arg Met, Cys-SH	Not obtainable[a]
O–Fe	Asn, Gln	
	Low-Spin[c]	
S^-–Fe–N	Cys, His	ArS^-, N-MeIm
	Cys, Lys(Arg)	ArS^-, RNH_2
S^-–Fe–S	Cys, Met	ArS^-, THT[f]
	Cys, Cys-H	ArS^-, ArSH
S^-–Fe–O	Cys, Asn(Gln)	ArS^-, DMF[g]
S–Fe–N	Met, His	[Cytochrome c][d]
O^-–Fe–N	Tyr, His	ArO^-, N-MeIm
	Ser(Thr), His	RO^-, N-MeIm
O^-–Fe–N,S,O	Tyr, Ser(Thr), Asp(Glu) Lys, Met, Asn(Gln)	high-spin[h]
N–Fe–N	His, His	N-MeIm, N-MeIm [Cytochrome b_5][e]

[a] Synthetic complexes corresponding to these ligation modes could not be isolated. [b] Biological example of Fe–N(His). [c] For other ligation cases generated in situ for EPR study cf. Table XIII. [d] Biological example of (Met)S–Fe–N(His). [e] Biological example of (His)N–Fe–N(His). [f] Tetrahydrothiophene. [g] *N,N*-Dimethylformamide. [h] EPR spectra reveal no low-spin signals using excess RNH_2, THT, DMF in the presence of high-spin complexes with L = ArO^-, RO^-, OAc^-. With the latter complex and N-MeIm $Fe(P)(N\text{-MeIm})_2^+$ was formed.

μ-oxo dimers affords a route to iron(II) porphyrins, and analytically pure Fe(PPIXDME) has been obtained in this way.[43] Upon exposure to air, ferric porphyrin thiolates in solution, with the exception of Fe(OEP)($SC_6H_4NO_2$), react immediately to give the μ-oxo dimer according to reaction 4. Iron(III) porphyrins with axial oxygen ligands are air-stable both as solids and in solution.

$$2Fe(P)(SAr) + \tfrac{1}{2}O_2 \rightarrow [Fe(P)]_2O + ArSSAr \quad (4)$$

High-Spin Complexes. The approach taken in assessing the various possible types of axial ligation modes in ox-P-450-S by use of synthetic porphyrin complexes is evident from Table V. Potentially coordinating amino acid residues are shown together with axial ligands intended as simulators of biological coordination. It is emphasized that not all conceivable ligation modes, based on the compositions of P-450 enzymes,[18] could be tested owing to failure to isolate or generate in solution the appropriate five-coordinate synthetic species. These cases are indicated, among which is $[Fe(P)(Im)]^+$. While a material corresponding to the composition Fe(PPIX)(Im)Cl has been described,[44] its solution properties are unknown. Consequently, acid-metHb and -Mb have been employed as "models" for Im(His) axial ligation in the substrate-bound enzyme. Using the known properties of these proteins and those of synthetic complexes described below, magnetic and spectroscopic features generated by three types of axial ligation are compared with those of ox-P-450-S, for which representative data are quoted.

(a) Structure of Fe(PPIXDME)($SC_6H_4NO_2$). The crystal structure consists of well-separated molecular units, with the shortest H···H intermolecular interaction being 2.35 Å. A stereoscopic view of the unit cell is presented in Figure 2. Given in Table VI is metrical information derived from the parameters of Tables I and II and from the inverse matrix. Various least-squares planes through portions of the molecule are presented in Table VII. The atomic numbering scheme employed is shown in Figure 3.

The $Fe^{III}N_4S$ coordination unit has the pyramidal configuration found in all high-spin iron(III) porphyrins,[37,38] but with marginally significant differences in Fe–N distances, which range from 2.042 (5) to 2.081 (5) Å and average to 2.064 Å. A stereoview of the molecule is given in Fig-

Table VI. Distances (Å) and Angles (deg) in Fe(PPIXDME)($SC_6H_4NO_2$)

Bond		Average	Type
Fe–N(1)	2.081 (5)	2.064 (18)[a]	$Fe–N_{porph}$
Fe–N(2)	2.042 (5)		
Fe–N(3)	2.074 (5)		
Fe–N(4)	2.057 (5)		
Fe–S	2.324 (2)		
S–C(35)	1.750 (7)		
N(1)–C(1)	1.384 (8)	1.382 (12)	$N–C_a$[b]
N(1)–C(4)	1.359 (7)		
N(2)–C(6)	1.379 (8)		
N(2)–C(9)	1.395 (8)		
N(3)–C(11)	1.383 (7)		
N(3)–C(14)	1.371 (7)		
N(4)–C(16)	1.397 (7)		
N(4)–C(19)	1.387 (7)		
C(1)–C(2)	1.455 (8)	1.438 (16)	$C_a–C_b$[c]
C(3)–C(4)	1.427 (9)		
C(6)–C(7)	1.436 (9)	1.451 (11)	$C_a–C_b$ "long"
C(8)–C(9)	1.418 (8)	1.425 (9)	$C_a–C_b$ "short"
C(11)–C(12)	1.462 (9)		
C(13)–C(14)	1.428 (8)		
C(16)–C(17)	1.449 (8)		
C(18)–C(19)	1.425 (8)		
C(2)–C(3)	1.343 (9)	1.352 (7)	$C_b–C_b$
C(7)–C(8)	1.358 (9)		
C(12)–C(13)	1.355 (8)		
C(17)–C(18)	1.350 (8)		
C(5)–C(4)	1.382 (9)	1.378 (12)	$C_m–C_a$[c]
C(5)–C(6)	1.371 (9)		
C(10)–C(9)	1.390 (9)		
C(10)–C(11)	1.367 (8)	1.388 (9)	$C_m–C_a$ "long"
C(15)–C(14)	1.384 (8)	1.367 (9)	$C_m–C_a$ "short"
C(15)–C(16)	1.360 (8)		
C(20)–C(19)	1.396 (8)		
C(20)–C(1)	1.370 (8)		
C(2)–C(21)	1.562 (10)	1.525 (26)	$C_b–C_{methyl}$
C(7)–C(24)	1.522 (9)		
C(12)–C(27)	1.508 (8)		
C(18)–C(34)	1.508 (8)		
C(3)–C(22)	1.491 (11)	1.489 (11)	$C_b–C_{vinyl}$
C(8)–C(25)	1.487 (10)		
C(22)–C(23)	1.102 (15)	1.18 (10)	Vinyl
C(25)–C(26)	1.248 (14)		
C(13)–C(28)	1.498 (9)		Propionic ester
C(17)–C(31)	1.495 (9)		
C(28)–C(29)	1.540 (9)		
C(31)–C(32)	1.533 (9)		
C(29)–C(30)	1.480 (10)		
C(32)–C(33)	1.499 (10)		
C(30)–O(1)	1.214 (9)		
C(30)–O(2)	1.296 (9)		
C(33)–O(3)	1.343 (9)		
C(33)–O(4)	1.197 (8)		
O(2)–Me(1)	1.500 (9)		
O(3)–Me(2)	1.451 (8)		
C(35)–C(36)	1.385 (9)	1.381 (17)	$C_{phenyl}–C_{phenyl}$
C(35)–C(40)	1.394 (8)		
C(36)–C(37)	1.380 (9)		
C(37)–C(38)	1.404 (9)		
C(38)–C(39)	1.357 (9)		
C(39)–C(40)	1.368 (9)		
C(38)–N(5)	1.481 (9)		
N(5)–O(5)	1.231 (9)		
N(5)–O(6)	1.198 (9)		
N(1)–Fe–N(2)	87.0 (2)		$FeN_4S_{polyhedron}$
N(1)–Fe–N(3)	156.0 (2)		
N(1)–Fe–N(4)	88.0 (2)		
N(2)–Fe–N(3)	87.9 (2)		
N(2)–Fe–N(4)	155.4 (2)		
N(3)–Fe–N(4)	87.0 (2)		

Bond		Average	Type
N(1)–Fe–S	101.1 (1)		
N(2)–Fe–S	104.3 (1)		
N(3)–Fe–S	103.0 (1)		
N(4)–Fe–S	100.3 (1)		
Fe–S–C(35)	100.4 (2)		
C(1)–N(1)–C(4)	107.2 (6)	105.7 (15)	$C_a–N–C_a$
C(6)–N(2)–C(9)	103.8 (6)		
C(11)–N(3)–C(14)	106.5 (5)		
C(16)–N(4)–C(19)	105.3 (5)		
N(1)–C(1)–C(2)	108.8 (6)	109.9 (12)	$N–C_a–C_b$
N(1)–C(4)–C(3)	109.1 (6)		
N(2)–C(6)–C(7)	111.3 (6)		
N(2)–C(9)–C(8)	111.3 (7)		
N(3)–C(11)–C(12)	108.5 (6)		
N(3)–C(14)–C(13)	110.7 (6)		
N(4)–C(16)–C(17)	108.8 (6)		
N(4)–C(19)–C(18)	110.9 (6)		
C(1)–C(2)–C(3)	106.0 (7)	107.2 (9)	$C_a–C_b–C_b$
C(2)–C(3)–C(4)	109.0 (7)		
C(6)–C(7)–C(8)	106.5 (7)		
C(7)–C(8)–C(9)	107.1 (7)		
C(11)–C(12)–C(13)	107.2 (6)		
C(12)–C(13)–C(14)	107.1 (6)		
C(16)–C(17)–C(18)	108.0 (6)		
C(17)–C(18)–C(19)	106.9 (6)		
N(1)–C(1)–C(20)	125.8 (6)	123.8 (13)	$N–C_a–C_m$
N(1)–C(4)–C(5)	123.0 (6)		
N(2)–C(6)–C(5)	123.4 (7)		
N(2)–C(9)–C(10)	122.3 (6)		
N(3)–C(11)–C(10)	125.6 (6)		
N(3)–C(14)–C(15)	123.0 (6)		
N(4)–C(16)–C(15)	124.2 (6)		
N(4)–C(19)–C(20)	123.0 (6)		
C(5)–C(4)–C(3)	127.9 (7)	126.3 (9)	$C_m–C_a–C_b$
C(5)–C(6)–C(7)	125.2 (7)		
C(10)–C(11)–C(12)	125.9 (6)		
C(10)–C(9)–C(8)	126.3 (7)		
C(15)–C(14)–C(13)	126.3 (6)		
C(15)–C(16)–C(17)	127.0 (6)		
C(20)–C(1)–C(2)	125.4 (7)		
C(20)–C(19)–C(18)	126.1 (6)		
C(1)–C(20)–C(19)	127.5 (6)	128.1 (7)	$C_a–C_m–C_a$
C(4)–C(5)–C(6)	128.5 (7)		
C(9)–C(10)–C(11)	127.9 (7)		
C(14)–C(15)–C(16)	128.3 (6)		
C(1)–C(2)–C(21)	122.8 (7)	124.3 (15)	$C_a–C_b–C_{alkyl}$
C(4)–C(3)–C(22)	122.7 (8)		
C(6)–C(7)–C(24)	124.6 (7)		
C(9)–C(8)–C(25)	123.8 (8)		
C(11)–C(12)–C(27)	124.5 (7)		
C(14)–C(13)–C(28)	127.4 (6)		
C(16)–C(17)–C(31)	123.8 (6)		
C(19)–C(18)–C(34)	124.4 (6)		
C(2)–C(3)–C(22)	128.2 (8)	128.5 (15)	$C_b–C_b–C_{alkyl}$
C(3)–C(2)–C(21)	131.2 (7)		
C(7)–C(8)–C(25)	129.2 (7)		
C(8)–C(7)–C(24)	128.8 (7)		
C(13)–C(12)–C(27)	128.3 (7)		
C(12)–C(13)–C(28)	125.6 (7)		
C(18)–C(17)–C(31)	128.2 (6)		
C(17)–C(18)–C(34)	128.7 (6)		
C(13)–C(28)–C(29)	112.8 (6)		Propionic ester
C(17)–C(31)–C(32)	110.6 (6)		
C(28)–C(29)–C(30)	113.4 (6)		
C(31)–C(32)–C(33)	112.7 (7)		
C(29)–C(30)–O(1)	125.7 (9)		
C(29)–C(30)–O(2)	113.1 (8)		
C(32)–C(33)–O(3)	110.8 (7)		
C(32)–C(33)–O(4)	126.0 (9)		

Table VI (*Continued*)

Bond		Average	Type
C(30)–O(2)–Me(1)	117.2 (8)		
C(33)–O(3)–Me(2)	116.1 (7)		
C(36)–C(35)–C(40)	118.1 (6)	120.0 (24)	C–C–C_{phenyl}
C(35)–C(36)–C(37)	122.3 (7)		
C(36)–C(37)–C(38)	116.7 (7)		
C(37)–C(38)–C(39)	122.5 (7)		
C(38)–C(39)–C(40)	119.2 (7)		
C(39)–C(40)–C(35)	121.2 (7)		
C(36)–C(35)–S	121.8 (6)		
C(40)–C(35)–S	120.2 (6)		
C(38)–N(5)–O(5)	117.0 (9)		
C(38)–N(5)–O(6)	118.5 (9)		
O(5)–N(5)–O(6)	124.4 (10)		

H···H Nonbonded Contacts <2.5 Å

H(1)C(40)···H(2)Me(2)	2.35
H(1)C(39)···H(2)C(32)	2.46

Signed Torsion Angles, deg

C(4)–C(3)–C(22)–C(23)	128 (2)
C(2)–C(3)–C(22)–C(23)	−50 (2)
C(7)–C(8)–C(25)–C(26)	−16 (2)
C(9)–C(8)–C(25)–C(26)	166 (1)
C(13)–C(28)–C(29)–C(30)	76 (1)
C(28)–C(29)–C(30)–O(1)	37 (1)
C(28)–C(29)–C(30)–O(2)	−142 (1)
C(29)–C(30)–O(2)–Me(1)	−179 (1)
C(17)–C(31)–C(32)–C(33)	−170 (1)
C(31)–C(32)–C(33)–O(4)	−7 (1)
C(31)–C(32)–C(33)–O(3)	174 (1)
C(32)–C(33)–O(3)–Me(2)	−175 (1)

Vector-Plane Angles, deg

Fe–N(1)	113.9 (3)
C(35)–C(37)–C(38)	
Fe–N(2)	105.5 (4)
C(35)–C(37)–C(38)	
Fe–N(3)	−90.1 (3)
C(35)–C(37)–C(38)	
Fe–N(4)	−98.6 (3)
C(35)–C(37)–C(38)	

[a] The figure in parentheses following an average value is the larger of that estimated for an individual value from the inverse matrix or on the assumption that the values averaged are from the same population. [b] The notation C_a, C_b, and C_m is that of J. L. Hoard, *Science*, 174, 1295 (1971). [c] See text for a discussion of long and short C_a–C_b and C_m–C_a bonds.

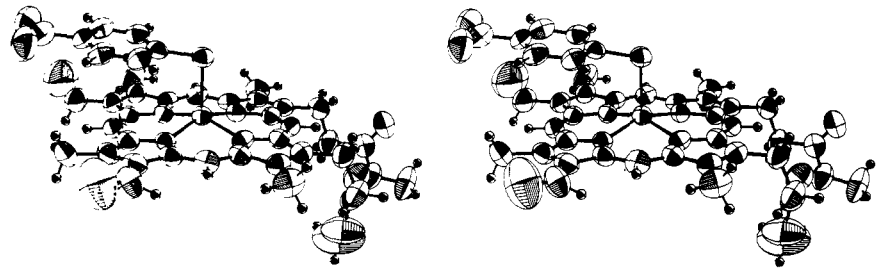

Figure 4. A stereoview of the molecule Fe(PPIXDME)($SC_6H_4NO_2$). Nonhydrogen atoms are drawn as 50% probability ellipsoids. Hydrogen atoms are drawn artificially small.

ure 4 and the coordination unit is depicted in Figure 5. The Fe atom is positioned 0.448 Å out of the 24-atom mean porphyrin plane and 0.434 Å out of the N_4 plane toward the axial sulfur atom. The porphyrin is accordingly "domed" toward the metal atom by 0.014 Å. The transannular N···N distances are 4.064 Å (N(1)-N(3)) and 4.005 Å (N(2)-N(4)) and hence the average Ct-N separation is 2.017 Å, although definition of the N_4 center (Ct)[37] is somewhat arbitrary where no symmetry is imposed on the N_4 unit. These values are in excellent agreement with the representative parameters for high-spin Fe(P)L complexes of Fe–N = 2.065 Å, Ct···N = 2.015 Å, and Ct···Fe = Fe···N_4 plane = 0.45 Å as given by Hoard.[37] The Fe–S distance of 2.324 (2) Å lies on the long end of the 2.21–2.31 Å range established in non-porphyrin high-spin ferric thiolate complexes,[45] and is ca. 0.11 Å longer than a low-spin Fe^{III}–SR interaction.[46] This distance is also ca. 0.07 Å longer than would be predicted from the difference in radii and the Fe–Cl distance in Fe(TPP)Cl.[38c] From Figure 4 it is seen that the $C_6H_4NO_2$ moiety is nearly parallel to the porphyrin ring and is situated in the region around C(5), on the opposite side of the ring from the bulky propionic ester groups. The dihedral angle between the phenyl and porphyrin rings is 11.1° (Table VII) and reflects in large measure the facts that the Fe–S vector is perpendicular to the porphyrin core and that the Fe–S–C(35) bond angle is 100.4 (2)°. The slight tipping of the phenyl ring is manifested in the distances of atoms C(35) through C(40) from the mean porphyrin plane; these distances are 3.09, 3.34, 3.58, 3.55, 3.30, and 3.12 Å, respectively. It is probable that the orientation of the phenyl ring with respect to the porphyrin skeleton results mainly from steric rather than electronic effects.[47] The bond distances and angles within the $SC_6H_4NO_2$ group are unexceptional. The distribution of distances within the phenyl ring suggests that the standard deviations assigned to the structure may be underestimated by a factor of 2. The bent axial bond and the locus of the phenyl ring, together with the marginally asymmetric placement of the Fe atom above the N_4 mean plane, degrades the metal site symmetry in the coordination unit from axial to rhombic.

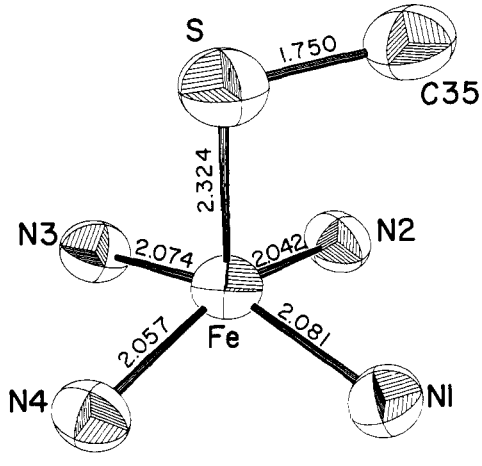

Figure 5. The inner coordination sphere of Fe(PPIXDME)($SC_6H_4NO_2$) showing principal distances and 50% probability ellipsoids.

As there are available authoritative reviews of porphyrin

Table VII. Deviations (Å), Interplanar Angles, and Equations of Weighted Least-Squares Planes[a]

	1	2	3	4	5	6	7
Fe	0.448	0.434					
S							−0.039
O(5)							−0.103
O(6)							−0.167
N(1)	−0.006 (5)	0.002 (5)	0.004 (5)				
N(2)	−0.005 (5)	−0.002 (5)		0.007 (5)			
N(3)	0.037 (5)	0.002 (5)			−0.007 (5)		
N(4)	0.029 (4)	−0.002 (5)				−0.010 (5)	
N(5)							−0.077
C(1)	0.055 (6)	0.062	−0.007 (6)				
C(2)	0.105 (7)	0.129	0.007 (7)				
C(3)	0.045 (7)	0.081	−0.003 (7)				
C(4)	−0.021 (6)	0.004	−0.003 (6)				
C(5)	−0.057 (6)	−0.026	0.027	0.008			
C(6)	−0.055 (6)	−0.033		−0.011 (6)			
C(7)	−0.043 (6)	−0.013		0.008 (6)			
C(8)	−0.023 (6)	−0.007		0.000 (6)			
C(9)	−0.008 (6)	−0.008		−0.008 (6)			
C(10)	0.002 (6)	−0.017		−0.030	0.003		
C(11)	0.025 (6)	−0.008			0.012 (6)		
C(12)	−0.012 (6)	−0.064			−0.010 (6)		
C(13)	0.023 (6)	−0.040			0.003 (6)		
C(14)	0.054 (6)	0.001			0.006 (6)		
C(15)	0.032 (6)	−0.027			−0.045	0.003	
C(16)	0.005 (6)	−0.044				0.014 (6)	
C(17)	−0.109 (6)	−0.165				−0.005 (6)	
C(18)	−0.117 (6)	−0.159				−0.004 (6)	
C(19)	−0.013 (5)	−0.040				0.012 (6)	
C(20)	0.036 (6)	0.027	−0.058			0.039	
C(21)	0.211						
C(22)	0.079						
C(23)	0.794						
C(24)	−0.016						
C(25)	−0.041						
C(26)	0.195						
C(27)	−0.044						
C(28)	0.021						
C(31)	−0.211						
C(34)	−0.269						
C(35)							−0.014 (5)
C(36)							0.005 (6)
C(37)							0.008 (7)
C(38)							−0.009 (6)
C(39)							−0.005 (6)
C(40)							0.016 (6)
Me(1)							
Me(2)							
Av dev	0.038	0.002	0.005	0.007	0.008	0.009	0.009

Angles between the Normals to the Planes[b]

Plane A	Plane B	Angle, deg	Plane A	Plane B	Angle, deg
1	2	0.8	3	6	6.4
1	3	3.0	3	7	10.1
1	4	1.3	4	5	2.1
1	5	1.3	4	6	4.5
1	6	3.8	4	7	12.4
1	7	11.1	5	6	4.9
1	8	54.7	5	7	10.6
1	9	14.2	6	7	11.0
3	4	3.6	3	8	51.7
3	5	1.7	4	9	15.5

Plane	A	B	C	D	Group
1	−6.574	−13.773	6.897	−1.567	Porphyrin
2	−6.474	−13.800	6.754	−1.523	Pyrrole N atoms
3	−6.124	−13.667	7.147	−1.453	Pyrrole 1
4	−6.445	−13.824	6.637	−1.524	Pyrrole 2
5	−6.379	−13.733	7.001	−1.406	Pyrrole 3
6	−7.348	−13.742	7.063	−1.699	Pyrrole 4
7	−7.139	−13.023	8.962	1.084	Phenyl
8	3.658	−6.765	7.257	0.567	Vinyl C(3), C(22), C(23)
9	−8.087	−12.800	9.359	−2.529	Vinyl C(8), C(25), C(26)

[a] The entries for which an error is not indicated are for atoms which were not included in the calculation of the plane. [b] The plane is in monoclinic coordinates as defined by W. C. Hamilton, *Acta Crystallogr.*, 18, 502 (1965).

Table VIII. Average Bond Lengths (Å) and Bond Angles (deg) in Two Ferric Protoporphyrin Complexes

Bond	Fe^{III}(PPIX) (N-MeIm)$_2$[a]	Fe^{III}(PPIXDME) ($SC_6H_4NO_2$)[b]
Fe···N	1.990 (16)	2.064 (18)
N–C_a	1.376 (8)	1.382 (12)
C_a–C_b	1.443 (22)	1.438 (16)
C_a–C_m	1.368 (19)	1.378 (12)
C_b–C_b	1.345 (10)	1.352 (7)
C_a–N–C_a	105.9 (14)	105.7 (15)
N–C_a–C_b	109.9 (12)	109.9 (12)
C_a–C_b–C_b	107.2 (12)	107.2 (9)
N–C_a–C_m	124.7 (10)	123.8 (13)
C_m–C_a–C_b	125.3 (8)	126.3 (9)
C_a–C_m–C_a	126.3 (8)	128.1 (7)

[a] Data from ref 39c. [b] This work.

Table IX. Magnetic and EPR Data for High-Spin Iron(III) Porphyrin Complexes

Complex	μ, BM[a]	g values
Fe(PPIXDME)($SC_6H_4NO_2$)	5.90[b]	[c]
Fe(PPIXDME)(SC_6H_4Cl)	5.87	7.2, 4.8, 1.9[d,e]
Fe(OEP)($SC_6H_4NO_2$)	5.92	[c]
Fe(OEP)(SPh)	5.87	7.2, 4.7, 1.9[d,f]
Fe(PPIXDME)($OC_6H_4NO_2$)	5.90	5.9, 2.0[e,g]
Fe(PPIXDME)(OEt)	5.88	6.5, 5.5, 1.9[d,f]
Fe(PPIXDME)(OAc)	5.87	5.9, 2.0[f,g]
Fe(OEP)(OMe)	5.94	6.0,[h] 1.9[f,g]
acid-met Mb, Hb	5.83[j]	5.9–6.0, 2.0[k]
ox-P-450$_{cam}$·S	5.2[i]	8.0, 4.0, 1.8[l]
Liver microsomal ox-P-450·S		8.1, 3.7, 1.7[m]
R. japonicum ox-P-450·S		7.9, 3.8, 1.8[n]

[a] 295 K; diamagnetic corrections were obtained from the reported value for H_2(PPIXDME) [R. Havemann, W. Haberditzl, and K.-H. Mader, *Z. Phys. Chem. (Leipzig)*, 218, 71 (1961)] and Pascal's constants. [b] $\chi_{corr}^{M} = 4.41/(T + 3.2)$ at $T = 20$–295 K. [c] Not measured due to insolubility in a suitable solvent. [d] Toluene glass. [e] ~5 K. [f] ~80 K. [g] DMF–CH_2Cl_2 (3:1 v/v) glass. [h] Broadening indicates small rhombic splitting. [i] 94–253 °C, ref 35a. [j] Reference 36. [k] References 58, 60, and 61. [l] Reference 51. [m] Reference 62. [n] Reference 63.

and metallorporphyrin geometries,[37] no detailed comparisons of the dimensions of the porphyrin skeleton with others in the literature are presented here. Comparisons are restricted to comparable data for the present structure and Fe(PPIX)(N-MeIm)$_2$,[39c] both of which involve the same porphyrin. The agreement between comparable parameters is excellent; the change from five to six coordination and from high spin to low spin appears to affect only the Fe–N bond lengths, within the accuracy of these determinations. In both structures and in that of mesoporphyrin IX dimethyl ester free base,[50] the vinyl groups are not coplanar with the porphyrin ring.

Although the average parameters in the porphyrin ring of Fe(PPIXDME)($SC_6H_4NO_2$) agree well with those expected from the considerable data for other porphyrin systems in the literature, the pattern of inequalities in the presumed equivalent C_a–C_b and C_a–C_m distances (Table VI) appears to be unique to the present structure. Proceeding around the periphery of the porphyrin core and examining first the eight C_a–C_b distances starting with C(1)–C(2), a long-short-long-short . . . pattern is evident. Similarly, from the eight C_a–C_m distances starting with C(4)–C(5) a similar pattern emerges. Combining these 16 distances one finds the long-short-long-short . . . alternation around the ring periphery, broken only by the apparent equivalence of the four C_b–C_b distances. Although this type of alternation might result from the unsymmetrical pattern of substitution on the protoporphyrin IX ring, an effect thus neither expected nor found in the symmetrical OEP and TPP derivatives, it was not observed in Fe(PPIX)(N-MeIm)$_2$.[39c] Even though there may be some underestimation of standard deviations of bond lengths in the present structure determination, the consistent alternating pattern is difficult to dismiss on this basis. Further diffraction studies on unsymmetrically substituted metalloporphyrins are required to corroborate or otherwise assess the observations made here.

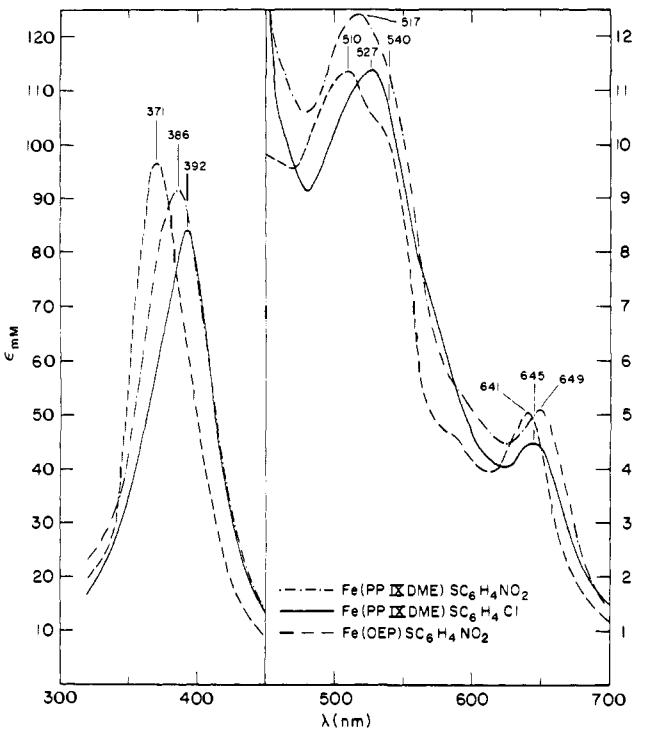

Figure 6. Electronic spectra of three Fe(III) porphyrin thiolates in dry dichloromethane solutions at ~25 °C.

(b) Magnetism. The data in Table IX show that all five-coordinate complexes are high-spin, including Fe(PPIXDME)($SC_6H_4NO_2$), which exhibits a T^{-1} susceptibility behavior from ambient temperature to 20 °K. Magnetic susceptibility,[35a] EPR,[51] and Mössbauer[52] results indicate that ox-P-450$_{cam}$·S in frozen samples at reduced temperatures exists as about 60–80% high-spin form obtained by substrate binding to the essentially pure low-spin resting state (eq 2). It has not yet been established whether stoichiometric substrate binding in solution leads to 100% high-spin form, but the lack of discernible low-spin features in the absorption spectra (vide infra) suggests that this is the case.

(c) Electronic Spectra. Visible absorption spectral data for Fe(PPIXDME)L complexes are collected in Table X and spectra of arylthiolate complexes in noncoordinating solvents are shown in Figure 6. All spectra are clearly of the high-spin type.[27,53] Those of thiolate complexes consist of an α band near or at 645 nm, a broad absorption in the β-band region containing a shoulder superimposed on a maximum at 517–534 nm, and a Soret band at 388–396 nm. Band positions and intensities exhibit a small dependence on the nature of the nonaqueous solvent. Spectra of OEP thiolates are included to show that these complexes are also high spin in solution, but cannot be employed for purpose of strict comparison with ox-P-450-S cytochromes. PPIXDME complexes with axial oxygen ligands (Figure 7) exhibit Soret and α-bands at 400–404 and 598–632 nm, respectively, in the solvents employed and thus are readily distinguished from the corresponding thiolate species. The same comment applies to acid-metMb and -Hb whose α-β-Soret band patterns, 630, 502, 408 nm and 631, 500, and 405

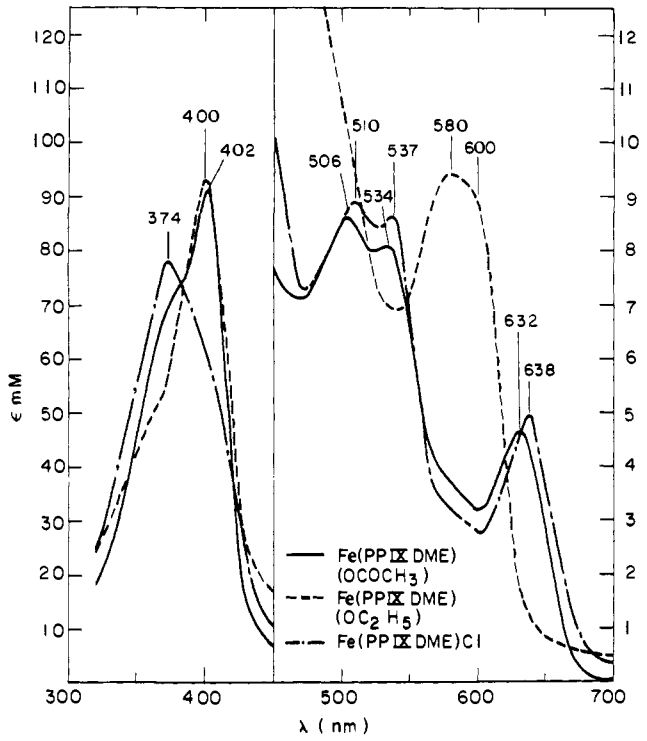

Figure 7. Electronic spectra of Fe(PPIXDME)(OAc) in HOAc-CH_2Cl_2 (1:19 v/v), Fe(PPIXDME)(OEt) in EtOH-CH_2Cl_2 (1:9 v/v), and Fe(PPIXDME)Cl in CH_2Cl_2 at ~25 °C.

nm,[54a] respectively, do not correspond closely in either band positions or intensities to those of Fe(PPIXDME)(SAr). Comparison of the spectral results for the latter complexes with those for the substrate-bound enzymes (Table X) reveals a striking similarity in α- and Soret band features. Comparisons in the β-band region are less useful inasmuch as spectral features are somewhat substrate dependent in the microsomal and mitochondrial enzymes and the β band in ox-P-450$_{cam}$·S is clearly a composite of several transitions.[8,11] Nonetheless, the thiolates do show a definite degree of spectral resemblance to the enzymes in this region. From these comparisons it is concluded that Fe(PPIXDME)(SAr) complexes are far more representative of the ox-P-450·S reaction state in terms of visible absorption spectra than are species containing axial N(Im) or anionic oxygen ligands.

(d) Magnetic Circular Dichroism Spectra. The MCD spectra of the preceding Fe(PPIXDME)L series of compounds have been obtained, and the full body of results will be published elsewhere.[55] Here it is noted that, whereas there is a high degree of similarity between the multi-featured spectra of the L = $SC_6H_4NO_2$ complex and ox-P-450$_{cam}$·S,[56] no such resemblance exists between the latter and complexes with axial oxygen ligands. These results also support sulfur coordination in the substrate-bound enzymes.

(e) EPR Spectra. Collected in Table IX and Figure 8 are EPR results for synthetic Fe(P)L complexes measured in glasses at either ~5 or ~80 K. All spectra are of the high-spin type.[57-59] Good quality spectra of Fe(P)($SC_6H_4NO_2$), P = PPIXDME and OEP, were not obtained owing to inadequate solubility in glass-forming solvents. Complexes with O- and N-donor axial ligands have either axial ($g_\perp = 6$, $g_\parallel = 2$) or near-axial (rhombic) symmetry, with the latter signaled by a splitting of the low-field resonance. The largest rhombic splitting observed for synthetic complexes of these types occurs with Fe(PPIXDME)(OEt), from whose spectrum the spin Hamiltonian parameter ratio E/D (vide infra) is 0.02, corresponding to ~6% rhombicity.[58] For Mbs and intact normal Hbs the degree of rhombicity is very small under normal conditions,[58,60,61] and reaches a value of 2.3% in one separated ferric α chain.[58,60] In contrast, the EPR spectra of Fe(PPIXDME)(SC_6H_4Cl) and Fe(OEP)(SPh) reveal relatively large rhombic distortions with $E/D \simeq 0.05$ or a rhombicity of 15%.

EPR spectra have been reported for numerous P-450 enzymes in the high-spin state. Some representative values[51,62,63] are summarized in Table IX, from which E/D = 0.083-0.092 and the degree of rhombicity is 25-28%. Although the preceding two Fe(P)(SAr) complexes do not attain the extent of ligand field rhombicity encountered with the enzymes,[64] only thiolates among the axial ligands tested produce substantial rhombic distortions. This point is emphasized by the axial spectrum of Fe(PPIXDME)($OC_6H_4NO_2$) compared with those of the thiolate complexes in Figure 8 and the rhombic spectrum of Fe(OEP)(SPh) whose porphyrin is axially symmetric. A poorly resolved spectrum of Fe(PPIXDME)($SC_6H_4NO_2$), also indicative

Table X. Electronic Spectral Data[a] for High-Spin Iron(III) Porphyrin Complexes

Complex	Solvent	λ_{max}, nm (ϵ_{mM})			
		α	β		γ (Soret)
Fe(PPIXDME)($SC_6H_4NO_2$)	Toluene	646 (4.8)	540 (sh, 10.4)	517 (11.2)	391 (86.8)
	CH_2Cl_2	649 (5.1)	540 (sh, 11.4)	517 (12.4)	386 (91.5)
	2-MeTHF[b]	647	540 (sh)	522	388
	Toluene/MeC_6H_{11}[c]	648	540 (sh)	522	390
Fe(PPIXDME)(SC_6H_4Cl)	Toluene	643 (4.4)	571 (10.4)	533 (11.5)	396 (83.3)
	CH_2Cl_2	645 (4.5)	565 (sh, 7.6)	527 (11.4)	392 (84.0)
	2-MeTHF	643	565 (sh)	534	396
Fe(OEP)($SC_6H_4NO_2$)	Toluene	640 (6.5)		512 (13.2)	374 (110)
	CH_2Cl_2	641 (5.0)	530 (sh, 10.5)	510 (11.4)	371 (96.6)
	2-MeTHF	642	530 (sh)	512	373
Fe(OEP)(SC_6H_5)	Toluene	634 (5.4)		520 (12.0)	385 (97.6)
	CH_2Cl_2	636 (5.0)		513 (11.7)	381 (101)
Fe(PPIXDME)($OC_6H_4NO_2$)	Toluene	617 (7.7)	528 (12.0)	500 (12.8)	404 (97.3)
	CH_2Cl_2	620 (9.0)	529 (13.5)	501 (15.0)	400 (102)
	2-MeTHF	616	528	498	403
Fe(PPIXDME)(OEt)	EtOH/CH_2Cl_2[d]	598 (sh, 9.3)	580 (9.4)	470 (sh, 15.3)	400 (92.7)
Fe(PPIXDME)(OAc)	HOAc/CH_2Cl_2[e]	632 (4.6)	534 (8.1)	506 (8.6)	402 (91.3)
ox-P-450$_{cam}$·S[f]	Aq	646 (4.5)	540 (sh, 10)	~520	391 (87)
Microsomal ox-P-450·S[g]	Aq	647	540 (sh)	517	394

[a] Ambient temperature. [b] 2-Methyltetrahydrofuran. [c] Toluene–methylcyclohexane (1:1 v/v). [d] 1:9 v/v. [e] 1:19 v/v. [f] References 8 and 11. [g] Reference 7b; see also ref 21 and 54b.

of appreciable rhombic splitting, was observed at ~5 K. Sources of EPR-detectable rhombicity in high-spin proteins have been considered[63] and the greater sensitivity of high-spin vs. low-spin EPR spectra to the effects of protein structure at all levels has been pointed out.[58] On this basis it is not surprising that the extent of departure from axial symmetry is greater in the enzymes than in the structurally unconstrained synthetic porphyrins.[64] Judging from x-ray results for Fe(PPIXDME)($SC_6H_4NO_2$), rhombicity in this and perhaps other thiolate complexes may be a ground state structural property, and may be accentuated by unequal interactions of sulfur lone pair orbitals with the spin-containing metal d_{xz}, d_{yz} orbitals. While recognizing that significant rhombicity exists in ferriheme proteins where sulfur ligation is not involved,[58,61] it is concluded that, within the limitations of synthetic complexes as models, the EPR data favor axial sulfur coordination in ox-P-450·S.

(f) Mössbauer Spectra and High-Field Magnetization Measurements. Spectral parameters for five-coordinate porphyrin complexes are given in Table XI and typical spectra at 4.2 and 77 K are set out in Figure 9. The spectra of all complexes are characterized by a single quadrupole doublet, the splitting and centroid of which vary little from 4.2 K to room temperature. As the temperature is raised, the symmetric doublet at 4.2 K becomes increasingly asymmetric as one component broadens. This behavior is similar to that observed with synthetic and biological ferrihemes[65-68] and has been interpreted in terms of electron spin relaxation which is fast at low temperatures and slower at higher temperatures because of thermal population of more slowly relaxing spin levels.[69] Isomer shifts (δ) and quadrupole splittings (ΔE_Q) for Fe(PPIXDME)($OC_6H_4NO_2$) and Fe(PPIXDME)($SC_6H_4NO_2$) are typical of high-spin $Fe^{III}N_4L$ complexes.

A comparison of the Mössbauer spectra of the heme complexes investigated shows that for Fe(PPIXDME)($OC_6H_4NO_2$) and Fe(PPIXDME)($SC_6H_4NO_2$) it is the higher energy absorption line that is broadened with increasing temperature. This indicates that the principal component of the electric field gradient tensor V_{zz} at the iron site is positive.[67] For Fe(PPIXDME)(OEt) the asymmetry is reversed, indicating a negative V_{zz}. This negative sign is also seen in the magnetically split Mössbauer spectra, discussed below. According to calculations by Sharma and Moutsos,[70] based on linear combinations of polarized atomic orbitals, an increase in the value of the polarizability of the axial ligand, with the polarizability of the in-plane ligands unchanged, decreases V_{zz} which eventually passes from a positive to a negative value. The experimental observation of a negative V_{zz} in Fe(PPIXDME)(OEt) can be understood on the basis of these calculations if the polarizability of OEt is assumed to be higher than that of $OC_6H_4NO_2$ or $SC_6H_4NO_2$.

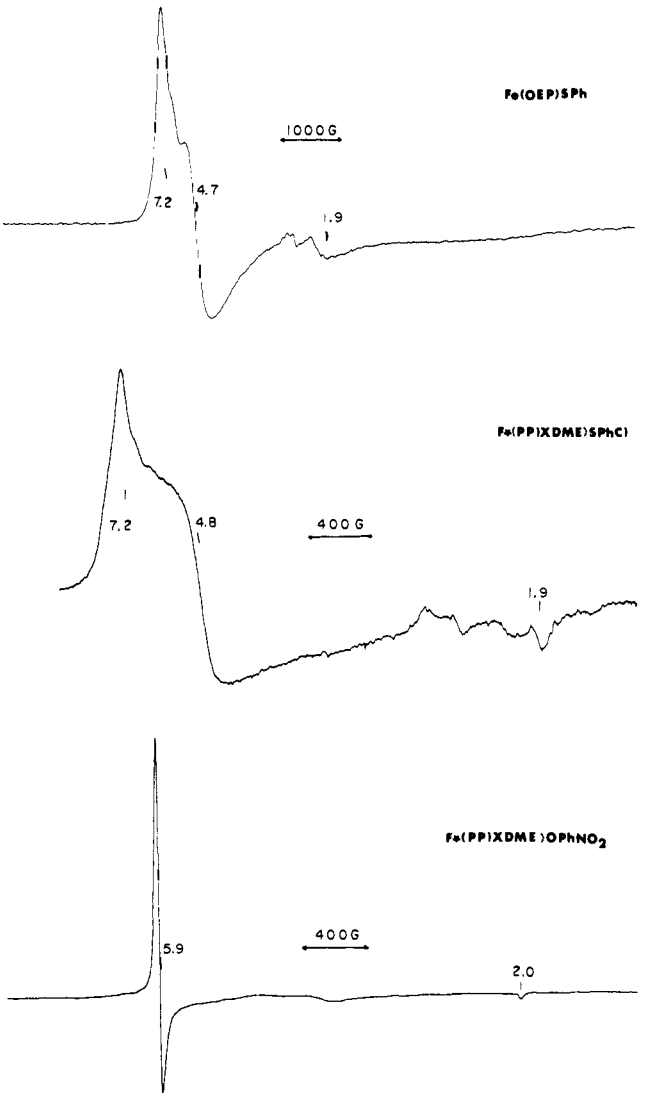

Figure 8. EPR spectra at ~80-95 K: Fe(OEP)(SPh) and Fe(PPIXDME)(SC_6H_4Cl) in toluene glasses, Fe(PPIXDME)($OC_6H_4NO_2$) in DMF-CH_2Cl_2 glass (3:1 v/v).

However, as these and other results[24,66-68] show, δ and ΔE_Q values exhibit no clear-cut dependence on the nature of either the in-plane tetraaza ligand or the axial ligand. Consequently, no conclusion can be drawn as to the nature of axial ligation in ox-P-450_{cam}·S, the only P-450 cytochrome studied by Mössbauer spectroscopy,[52] on the basis of the δ and ΔE_Q data in Table XI. Spectra in external magnetic fields, as well as magnetization measurements, were obtained and analyzed in an attempt to develop useful criteria for identification of axial ligands in the PPIXDME

Table XI. Mössbauer Data for High-Spin Iron(III) Porphyrin Complexes

Compd	δ, mm/s[a,b]	ΔE_Q, mm/s[b]	$H_{hf}°$, kOe[b]	D, cm^{-1}
Fe(PPIXDME)($SC_6H_4NO_2$)	0.33 ± 0.03	0.76 ± 0.05	−476 ± 10	$10 \leqslant D \leqslant 12$
(CH_2Cl_2 soln)	0.32 ± 0.03	0.88 ± 0.05		
Fe(OEP)(SPh)	0.31 ± 0.03	0.49 ± 0.05		
Fe(PPIXDME)($OC_6H_4NO_2$)	0.30 ± 0.03	0.74 ± 0.05	−495 ± 5	6.6 ± 0.2
(CH_2Cl_2 soln)	0.33 ± 0.03	0.98 ± 0.05		
Fe(PPIXDME)(OEt)	0.32 ± 0.03	0.46 ± 0.05	−522 ± 8	5.3 ± 0.2
Fe(OEP)(OMe)	0.34			
Acid-metMb[c,d]	0.4	1.3	−498 ± 4	9.5 ± 1.5[g]
Fe(PPIX)(Im)Cl[e]	0.26	0.78		
Fe(PPIX)Cl[c]	0.35	0.75	−480	7
ox-P-450_{cam}·S[f]	0.35	0.79	−448 ± 10	3.8[h]

[a] Relative to Fe metal. [b] Values at 4.2 K unless otherwise specified. [c] 195 K. [d] Reference 66a. [e] Reference 44. [f] Reference 52, 200 K. [g] Reference 97. [h] Reference 51.

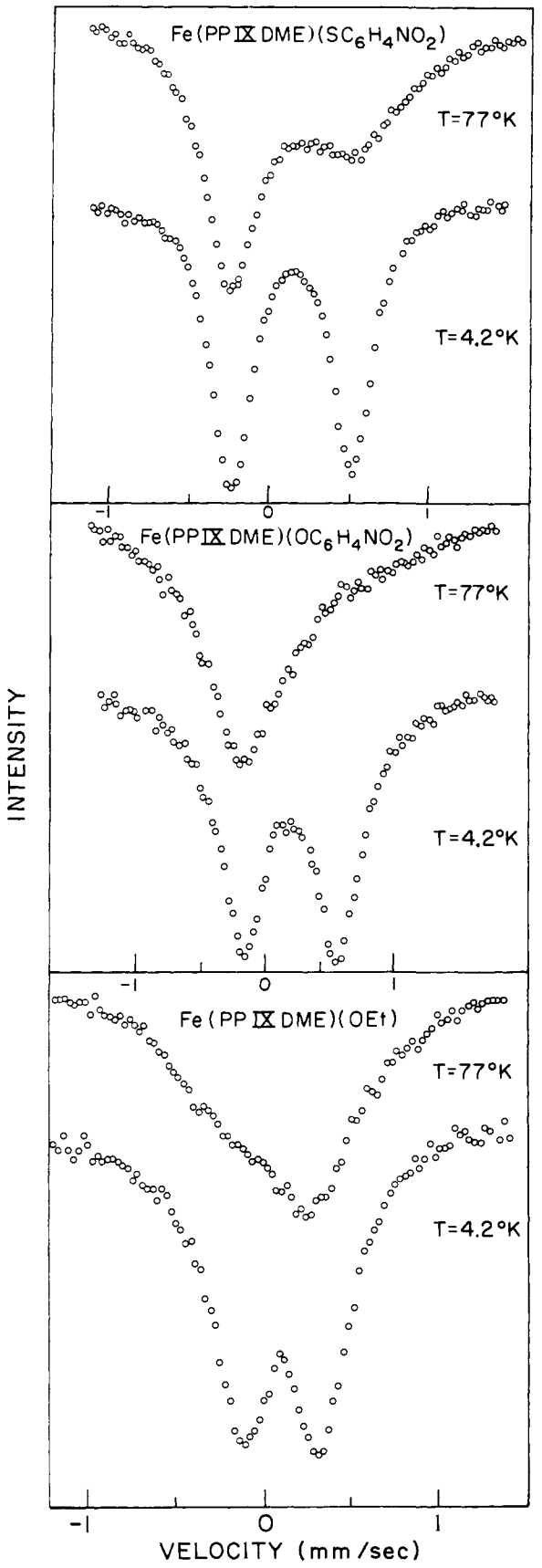

Figure 9. Zero-field Mössbauer spectra of three high-spin iron(III) porphyrins at 4.2 and 77 K.

series. These criteria are based on the effect of the axial ligand on the zero-field splitting and magnetic hyperfine structure constant of the Fe^{3+} ion.

(i) **Theory.** In the presence of a low-symmetry crystalline field the six-fold spin degeneracy of the Fe^{3+} ground electronic state, $^6A_1$, is partially lifted via the spin–orbit interaction with higher excited states.[57,71] Through the same interaction the isotropic magnetic hyperfine tensor expected for a d^5 shell, arising primarily from the Fermi contact interaction, becomes anisotropic.[66] The magnetic hyperfine interaction of the electronic spin with the nuclear moment corresponds to fields of the order of 10 G acting upon the electrons. In applied magnetic fields large compared with this, the electronic state of the iron ion can be determined by the electronic part of the Hamiltonian alone; i.e., the hyperfine terms may be neglected.[72] In the spin Hamiltonian formalism,[73] the electronic terms may be written as

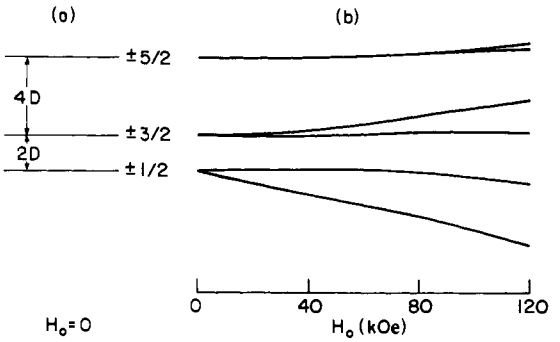

Figure 10. Energy level diagram for the ground state of Fe^{3+}, $^6A_1$, in (a) zero magnetic field and (b) as a function of applied field H_0 perpendicular to the z axis for $D = 7\ cm^{-1}$ and $E = 0$.

$$H_e = D[S_z^2 - \tfrac{1}{3}S(S+1)] + E(S_x^2 - S_y^2) + 2\beta\mathbf{H}_0 \cdot \mathbf{S} \quad (5)$$

where $\mathbf{H}_0$ is the applied magnetic field and S is the electronic spin. The zero-field splitting constant D gives a measure of the axial component of the crystalline field at the iron site and determines the energy separation between the Kramer's doublets of the $|S = \frac{5}{2}\rangle$ ground state of Fe^{3+} as shown in Figure 10a. The second term in eq 5 takes into account rhombic distortions of the crystalline environment and results in small admixtures of the $|\pm\frac{3}{2}\rangle$ and $|\pm\frac{5}{2}\rangle$ states into the ground state. The last term gives the Zeeman interaction of the electrons with the applied magnetic field which further mixes and splits the three Kramer's doublets. We have calculated the variation of the eigenvalues and eigenfunctions of the Hamiltonian of eq 5 as a function of $\mathbf{H}_0$ for various values of D and E. The resulting electronic energy level scheme of the Fe^{3+} ground state is shown as a function of the applied magnetic field $\mathbf{H}_0$ parallel to the heme plane, for the case of an axially symmetric crystalline field ($E = 0$) in Figure 10b.

The nuclear part of the magnetic hyperfine Hamiltonian is given by

$$H_N = -g_N\mu_N\mathbf{I} \cdot \mathbf{H}_0 + \mathbf{I} \cdot A \cdot \mathbf{S} \quad (6)$$

where the first term gives the nuclear Zeeman interaction with the applied field and the second the hyperfine interaction of the electronic spin with the nuclear moment. The electron spin operator in eq 6 may be replaced by its average value

$$\langle \mathbf{S} \rangle = \sum_{i=1}^{6} \langle \alpha_i | S | \alpha_i \rangle e^{-E_i/kT} \Big/ \sum_{i=1}^{6} e^{-E_i/kT} \quad (7)$$

where the summation goes over the eigenstates of Hamiltonian (eq 5) with the sixfold spin multiplet of the $S = \frac{5}{2}$ ground state taken as the basis set. Furthermore, in a strong axial crystalline field observed in most spin ferric porphyrins ($g_\perp > g_\parallel$ relative to a $S = \frac{1}{2}$ spin Hamiltonian) the electron spins tend to align in the plane perpendicular to the

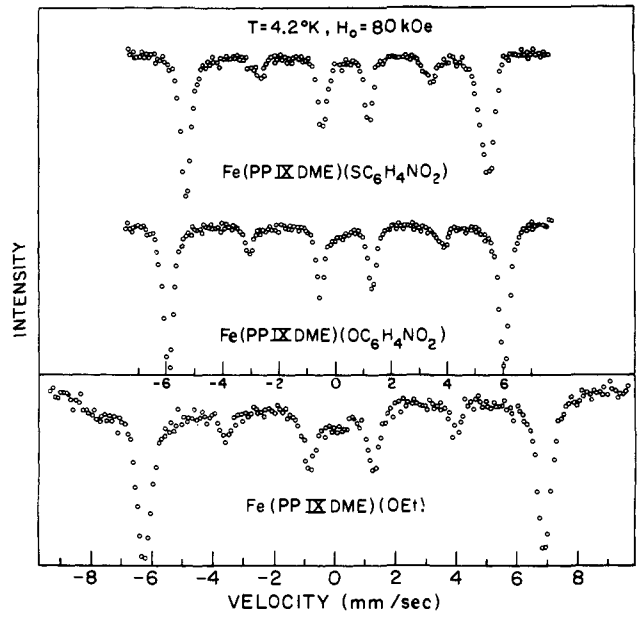

Figure 11. Mössbauer spectra of three high-spin iron(III) porphyrins at 4.2 K in a longitudinal magnetic field of 80 kOe.

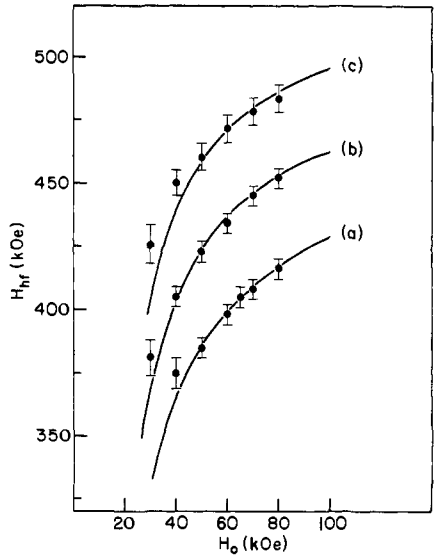

Figure 12. Observed hyperfine magnetic fields at 4.2 K and best theoretical fits to the experimental data for: (a) Fe(PPIXDME)($SC_6H_4NO_2$), D = 10 cm^{-1}, H_{hf}^0 = −476 kOe; (b) Fe(PPIXDME)($OC_6H_4NO_2$), D = 6.6 cm^{-1}, H_{hf}^0 = −495 kOe; (c) Fe(PPIXDME)(OEt), D = 5.3 cm^{-1}, H_{hf}^0 = −523 kOe.

z axis.[74,75] Thus $\langle \mathbf{S} \rangle$ lies in the heme plane and has a magnitude largely independent of the orientation of $\mathbf{H}_0$ relative to the z axis. As shown by previous investigators,[76] for angles of the applied field $\mathbf{H}_0$ with respect to the z axis greater than 30°, $\langle \mathbf{S} \rangle$ reaches its maximum value and lies in the heme plane. This fact, coupled with the high statistical probability for the magnetic field to lie in the heme plane, is responsible for the observation of well-resolved, magnetically split Mössbauer spectra in polycrystalline samples in an external magnetic field. Consequently we may rewrite eq 6 as

$$H_N = -g_N\mu_N \mathbf{I} \cdot \mathbf{H}_0 + A_\perp \langle \mathbf{S}_\perp \rangle \cdot (\mathbf{I}_x + \mathbf{I}_y) \qquad (8)$$

where only the components of the spin and the magnetic hyperfine tensor in the heme plane are considered.

The second term of eq 8 can be treated as an effective magnetic field at the nucleus by combining it with the Zeeman term to give

$$H_N = -g_N\mu_N \mathbf{I} \cdot \left[\mathbf{H}_0 - \frac{A_\perp \langle \mathbf{S}_\perp \rangle}{g_N\mu_N} \right] \qquad (9)$$

We may then define an effective magnetic field acting at the nucleus by

$$\mathbf{H}_{eff} = \mathbf{H}_0 + \mathbf{H}_{hf} \qquad (10)$$

where

$$\mathbf{H}_{hf} = H_{hf}^0 [\langle \mathbf{S}_\perp \rangle / S] \qquad (11)$$

$\langle \mathbf{S}_\perp \rangle / S$ gives the expectation value of the spin as a fraction of its saturation value $S = \frac{5}{2}$ and $H_{hf}^0 = -5A_\perp / 2g_N\mu_N$ is the saturation magnetic hyperfine field or the magnetic hyperfine structure constant, a parameter expected to be sensitive to the nature of the axial ligand of the metalloporphyrin compounds. Typically, for high-spin Fe^{3+} this constant is of the order of −520 kOe.

Since the Mössbauer spectrum in an external magnetic field is determined in general by three constants, D, E, and H_{hf}^0, magnetic moment measurements in high magnetic fields that can give information on the values of D and E were also undertaken. The theory is similar to that outlined above starting with eq 5, except that the magnetization measurements involve the moment induced parallel to the external field direction.

To obtain the magnetic moment per iron atom one must calculate matrix elements of the form $\langle \alpha | \mu_B(\mathbf{L} + 2\mathbf{S}) | \alpha \rangle$ where $|\alpha\rangle$ are eigenstates of the Hamiltonian of eq 5 and μ_B the Bohr magneton. For the case under consideration the orbital angular momentum is quenched, i.e., $\mathbf{L} = 0$, and the matrix elements to be calculated are reduced to $2\mu_B \langle \alpha | S | \alpha \rangle$. The observed magnetization at temperature T is given by the thermal average of this quantity according to eq 7, projected onto the direction on the magnetic field $\mathbf{H}_0$. Furthermore, for a powder sample a spatial average over all directions of the magnetic field is required[77] and was carried out numerically. To ascertain convergence of the summation the same calculation was performed for different numbers of discretely selected angles θ_i and ϕ_i where θ and ϕ determine the direction of $\mathbf{H}_0$ relative to the crystalline axes, with ϕ being the azimuthal angle. For the range of the parameter values used angular increments of $\Delta\theta = 2°$ and $\Delta\phi = 10°$ were sufficient to obtain convergent results.

(ii) Results. Typical magnetically split Mössbauer spectra obtained for Fe(PPIXDME)($OC_6H_4NO_2$), Fe(PPIXDME)($SC_6H_4NO_2$), and Fe(PPIXDME)(OEt) are shown in Figure 11. Experimental data were obtained over a range of applied field strengths from 20 to 80 kOe parallel to the γ-ray direction, and the effective magnetic field at the nucleus was obtained from the overall splitting of the outer absorption lines. Below 30 kOe, most samples gave poorly resolved broad-line spectra. The presence of vestigal $\Delta m = 0$ lines in these spectra arises because the induced spin is not exactly parallel to $\mathbf{H}_0$. The position of those lines is determined by the magnitude and sign of ΔE_Q and, in addition, by the relative orientation of the induced spin and V_{zz}, the principal component of the electric field gradient tensor. In all these cases, V_{zz} is perpendicular to the heme plane while $\langle S \rangle$ is induced in the heme plane. However, whereas V_{zz} is positive for Fe(PPIXDME)($OC_6H_4NO_2$) and Fe(PPIXDME)($SC_6H_4NO_2$), the negative sign for V_{zz} in Fe(PPIXDME)(OEt) results in the centroid of the $\Delta m = 0$ lines being shifted in the opposite direction relative to the outer lines, compared with the former two compounds.

In Figure 12 H_{hf} is plotted as a function of applied magnetic field for spectra obtained at 4.2 K. The solid curves are theoretical, calculated from eq 5, 7, 10, and 11.[78] The values of D and E were obtained from the results of mag-

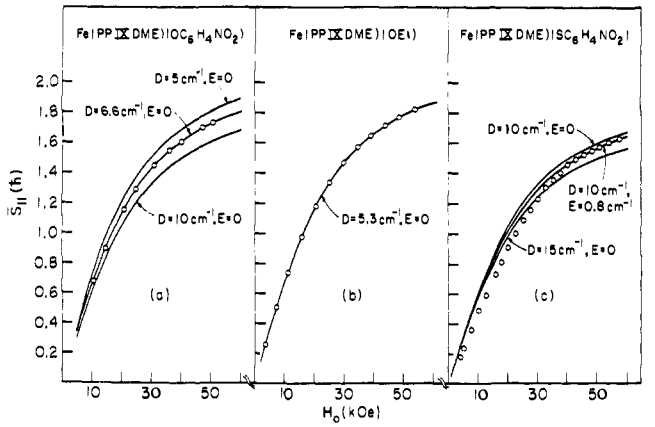

Figure 13. (a) Magnetization data and theoretical fit at 4.2 K for Fe(PPIXDME)($OC_6H_4NO_2$). Theoretical curves for D = 5 and 10 cm^{-1} are also shown for comparison. The magnetic moment in μ_B/Fe atom is given by $2\bar{S}_{\parallel}$. (b) Magnetization data and theoretical fit for Fe(PPIXDME)(OEt) at 4.2 K. (c) Magnetization data for Fe(PPIXDME)($SC_6H_4NO_2$) at 4.2 K and theoretical plots for different values of D and E. At low H_0 the experimental points are consistently lower than any reasonable values of D and E would predict.

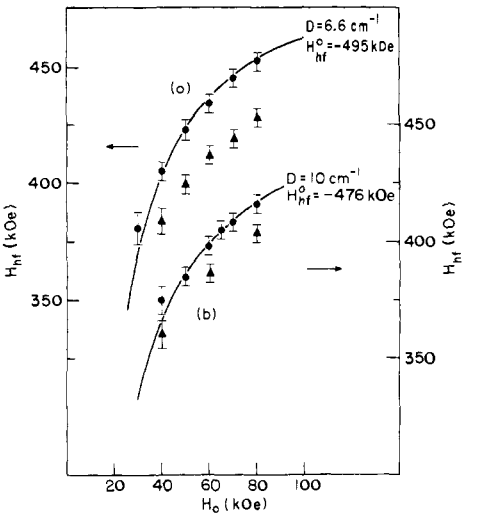

Figure 14. Experimental H_{hf} data for (a) Fe(PPIXDME)($OC_6H_4NO_2$) and (b) Fe(PPIXDME)($SC_6H_4NO_2$) in polycrystalline powders (●) and frozen dichloromethane solutions (▲) at 4.2 K.

netization measurements, and thus the fits serve to determine values of H_{hf}^0, which are tabulated in Table XI. As noted below, good fits were obtained to the magnetization data for Fe(PPIXDME)($OC_6H_4NO_2$) and for Fe(PPIXDME)(OEt). For Fe(PPIXDME)($SC_6H_4NO_2$) a good fit over the whole field range was not obtained, so the value of D used to compute the curve in Figure 12 for this case was taken from the best fit to the magnetization data obtained over the same field range, i.e., for $H_0 \geq 40$ kOe. The resultant uncertainty in the value of D results in a larger probable error for H_{hf}^0 in this case.

In Figure 13 the induced spin per iron atom (equal to ½ the magnetic moment) is plotted as a function of applied field for Fe(PPIXDME)($OC_6H_4NO_2$), Fe(PPIXDME)(OEt), and Fe(PPIXDME)($SC_6H_4NO_2$). In the first case, Figure 13a, the best fit with $D = 6.6 \pm 0.2$ cm^{-1} is shown, together with the theoretical curves for D = 5 and 10 cm^{-1} to indicate the sensitivity of the measurements to the magnitude of this parameter. In this case, $E = 0$, in agreement with the EPR results which show $E/D \simeq 0$, i.e., axial symmetry. A good fit is also obtained in Figure 13b with $D = 5.3 \pm 0.2$ cm^{-1}, and $E = 0$. As can be seen in Figure 13c we were unable to obtain, within the above spin Hamiltonian formalism, a good fit to the experimental data for Fe(PPIXDME)($SC_6H_4NO_2$) over the whole range of magnetic field strengths used. For the related complex Fe(PPIXDME)(SC_6H_4Cl), EPR measurements show nonaxial zero-field splitting with $E/D \simeq 0.05$. For fields ≥40 kOe (used for the Mössbauer work) a good fit could be obtained for $D = 10$ cm^{-1} and $E = 0.8$ cm^{-1}, but values of $10 \leq D \leq 12$ cm^{-1} and $E \leq 0.8$ cm^{-1} also gave reasonable results. With lower values of H_0, however, the observed magnetization was consistently lower than that calculated for all reasonable values of the parameters D and E. This discrepancy might be due to the oversimplified spin Hamiltonian used or to sample impurities. Inclusion of contributions from quartic order terms $S_x^4 + S_y^4 + S_z^4$ in the spin Hamiltonian might have improved somewhat the agreement between theory and experiment, but the effect of these terms is known to be small.[73] Nevertheless, the overall magnitude of the zero-field splitting obtained from the magnetization measurements of these compounds is consistent with the Mössbauer data and gives confidence in the magnitudes of the values of H_{hf}^0 obtained.

The Mössbauer parameters obtained for ox-P-450_{cam}·S are listed in Table XI with those of several other high-spin heme complexes for comparison. As noted above, isomer shifts and quadrupole splittings alone do not discriminate among axial ligands. The magnetic hyperfine interaction constant, however, is sensitive to the nature of the axial ligand. For example, we have concluded from our results that anionic oxygen ligation results in $H_{hf}^0 > -500$ kOe. Another possibility in the cytochrome is nitrogen ligation; measurements of acid-metMb have yielded $H_{hf}^0 \sim -500$ kOe. Thus, of the experimentally accessible and biologically viable alternatives, only thiolate sulfur coordination (in Fe(PPIXDME)($SC_6H_4NO_2$)) gives a value of H_{hf}^0 significantly below −500 kOe and approaching that in ox-P-450_{cam}·S. This result, together with the EPR evidence that oxygen ligation produces small or zero rhombicity whereas sulfur ligation results in a substantial rhombic distortion, points to thiolate sulfur as the axial ligand in the ox-P-450·S reaction state.

In order to investigate the possible constraints imposed by the crystalline environment in the solid compounds, Mössbauer spectra were obtained for Fe(PPIXDME)($OC_6H_4NO_2$) and Fe(PPIXDME)($SC_6H_4NO_2$) in frozen solutions in nonpolar solvents. The parameters obtained in frozen dichloromethane solutions are included in Table XI. In both cases, δ is virtually unchanged by solution, the quadrupole splitting increases, and H_{hf} decreases (Figure 14). As discussed above, the magnitude of H_{hf} depends on D, E, and H_{hf}^0, and a decrease in H_{hf} could reflect a decrease in H_{hf}^0 or an increase in D and E. Previous investigators[67,68] have noted that for hemin derivatives with different axial ligands, the magnitudes of ΔE_Q and D are qualitatively correlated, with larger ΔE_Q going with larger D. However, to our knowledge, this correlation has not been made for a single species in various solvents. Thus, in the absence of magnetization measurements of the solution samples, we can say at present that the electronic properties are dependent on the particular environment, and thus the unique parameters observed in the ox-P-450·S state reflect in part the protein environment of the prosthetic group.

Low-Spin Complexes. Various modes of axial ligation in low-spin six-coordinate complexes, used as test cases for the resting enzyme reaction state, ox-P-450, have been introduced by two methods. The first involves the base adduction reaction shown in Figure 1 starting from an *isolated* five-coordinate Fe(P)L species, and leads to the formation of Fe(P)LL′ in which L = ArS^-, ArO^-, OAc^-, and OR^-. The

approach is outlined in Table V where potential biological coordinating residues and their synthetic counterparts are evident. The second method also utilizes in situ generation of Fe(P)LL′, but by cleavage of a μ-oxo dimer with HL in the presence of a base L′. When the reactants are rapidly mixed at ambient temperature and the reaction mixture quickly quenched at low temperature the six-coordinate complexes are readily detectable by EPR. In this way the effects of axial ligands, such as alkylthiolates, thiols, thioethers, primary amines, and amides, can be examined. Nearly all species produced in this manner contain one anionic ligand. The ligation mode corresponding to (Met)S-Fe-N(His) was not obtainable by this procedure and recourse was taken to certain properties of ferricytochrome *c*, for which this type of axial coordination has been established by x-ray diffraction.[79,80] The complex $[Fe(PPIXDME)(N\text{-}MeIm)_2]^+$ was prepared by the reaction of N-MeIm with Fe(PPIXDME)Cl in solution as a model for (His)N-Fe-N(His) axial coordination, a biological example of which has been structurally established in cytochrome b_5.[81]

In view of the results obtained with high-spin complexes, isolation of a complex of the type Fe(P)(SR)L′ is a matter of importance. Our attempts to do so have thus far been unsuccessful. EPR monitoring of appropriate reaction mixtures with a variety of ligands L′ has shown that, after the initial low-temperature quench, further thaw–quench cycles were accompanied by rapid decrease in the intensity of the low-spin Fe(III) set of rhombic signals (vide infra) with no other resonance detectable at 80–95 K. Available evidence indicates spontaneous decomposition by reaction of eq 12, as noted by others[23,26] who have also achieved in situ gener-

$$2Fe^{III}(P)(SR)L' + 2L' \rightarrow 2Fe^{II}(P)L_2' + RSSR \quad (12)$$

ation of low-spin thiolate species. This reaction, as (3), may be preventable by thwarting radical coupling as, e.g., in the reported immobilization and attendant stability of iron(III) thiolate complex on a polymer support.[26] Because of the instability of six-coordinate species and in some cases the lack of complexation (Table V), the scope of physical studies of these complexes is less extensive than for five-coordinate complexes.

(**a**) **Electronic Spectra.** When various Fe(P)L complexes were exposed to an array of potential ligands L′ in solution at ambient temperature, either no reaction occurred (cf. Table V) or the redox process of eq 12 ensued. Satisfactory spectra of Fe(P)LL′ complexes could be obtained only in glass media at low temperatures and only with certain combinations of L and L′. Relevant spectra and spectral data

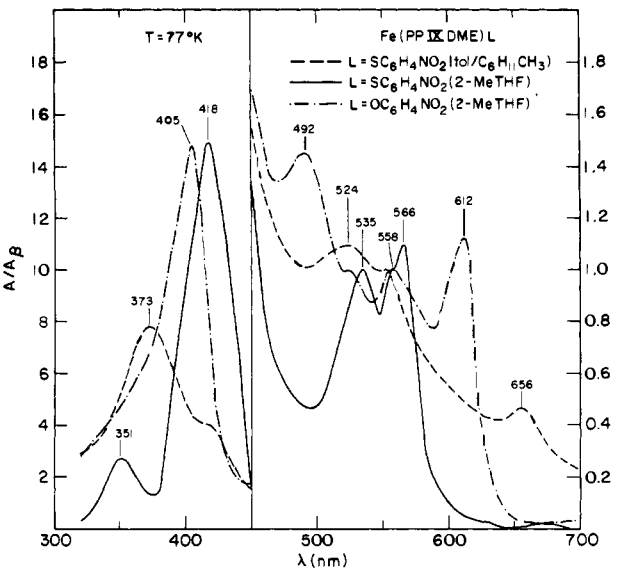

Figure 15. Electronic spectra of five- (- - -) and six-coordinate (—, • - • -) PPIXDME complexes in the indicated glasses at 77 K. Both absorbance scales correspond to the ratio A/A_β (cf. Table XII).

are given in Figure 15 and Table XII. In 2-MeTHF solution at ~25 °C Fe(PPIXDME)($SC_6H_4NO_2$) exhibits a high-spin spectrum (Table X). Upon cooling to 77 K the spectrum changed to that of a low-spin ferric heme complex,[53] formulated as Fe(PPIXDME)($SC_6H_4NO_2$)(2-MeTHF), with absorption maxima at 418, 535, and 566 nm. High-spin/low-spin conversion is fully reversible as shown by spectral monitoring through an additional cycle of temperature change. The spectra in Figure 15 reveal the difference between the five - and six-coordinate forms of the *p*-nitrobenzenethiolate complex at 77 K. The spectrum of the former shows appreciable α and Soret band shifts compared with its ambient temperature solution spectrum (Figure 6, Table X). Also evident from Figure 15 is the failure of the *p*-nitrophenolate complex to form a 2-MeTHF adduct. Numerous other attempts to obtain the spectra of low-spin complexes, utilizing very dilute solutions, rapid mixing techniques at and below room temperature, and immediate low-temperature quenching, were not successful. The system Fe(PPIXDME)($SC_6H_4NO_2$)/N-MeIm, in particular, was the object of considerable experimentation, but the only reaction product that could be identified by absorption spectral measurements was the Fe(II) complex Fe(PPIXDME)(N-MeIm)$_2$. These results discouraged attempts to obtain Mössbauer spectra of six-coordinate complexes.

Table XII. Electronic Spectral Data for Low-Spin Iron(III) Porphyrin Complexes

Complex	Solvent		λ_{max}, nm		
			α	β	γ (Soret)
Fe(PPIXDME)($SC_6H_4NO_2$)(2-MeTHF)[a,b]	2-MeTHF[c]	678 (0.02)	566 (1.1)	535 (1.0)	418 (14.9)
Fe(PPIXDME)($SC_6H_4NO_2$)(DMF)[a,b]	Toluene/MeC_6H_{11}[d]	683 (0.03)	567 (1.1)	533 (1.0)	420 (14.1)
Fe(PPIXDME)(SC_6H_4Cl)(2-MeTHF)[a,b]	2-MeTHF	684 (0.02)	566 (1.0)	536 (1.0)	422 (14.2)
Fe(OEP)($SC_6H_4NO_2$)(2-MeTHF)[a,b]	2-MeTHF	672 (0.08)	556 (1.2)	526 (1.0)	407 (13.0)
$[Fe(PPIXDME)(N\text{-}MeIm)_2]^+$[e]	CH_2Cl_2		558 (sh)	532	409
Cytochrome b_5[e,k]	Aq		560	532	413
Fe(PPIXDME)($OC_6H_4NO_2$)[a,b,f]	2-MeTHF	612 (1.1)	558 (1.0)	525 (0.99) 492 (1.4)	405 (14.8)
Fe(PPIXDME)($SC_6H_4NO_2$)[a,b,f]	Toluene/MeC_6H_{11}[d]	656 (0.5)	553 (1.0)	524 (1.1)	373 (7.8)
ox-P-450$_{cam}$[e,g,h]	Aq		571 (10.5)	535 (10)	417 (105)
ox-P-450$_{LM}$[l,h,i]	Aq		568 (14.2)	534 (13.6)	417 (124)
Mitochondrial ox-P-450[j]	Aq[e]		569	535	417
	Aq[a]		567	532	416

[a] 77 K. [b] Values in parentheses are the absorbance ratios A/A_β. [c] 2-Methyltetrahydrofuran. [d] Toluene–methylcyclohexane (1:1 v/v) with DMF added. [e] Ambient temperature. [f] High-spin. [g] References 8 and 11. [h] ϵ_{mM} in parentheses. [i] Reference 13b. [j] Reference 54b. [k] Pig liver; R. Bois-Poltoratsky and A. Ehrenberg, *Eur. J. Biochem.*, 2, 361 (1967).

Table XIII. EPR Spectra of Low-Spin Iron(III) Porphyrin Complexes Fe(P)LL'

Fe(P)L[a]	Base(L')	g values[b]			Fe(P)L[a]	Base(L')	g values[b]		
	S⁻-Fe-N				Fe(PPIXDME)(SCH_2Ph)[c]	DMF[e]	2.36	2.24	1.95
Fe(PPIXDME)($SC_6H_4NO_2$)	N-MeIm	2.42	2.26	1.91	Fe(PPIXDME)($SC_6H_4NO_2$)	2-MeTHF[d] or THF	2.36	2.26	1.94
	N-MeIm (2-MeTHF[d])	2.44	2.27	1.90					
Fe(PPIXDME)($SC_6H_4NO_2$)[c]	N-MeIm	2.43	2.27	1.91	Fe(PPIXDME)(SCH_2Ph)[c]	THF	2.29	2.22	1.97
Fe(PPIXDME)(SC_6H_4Cl)	N-MeIm	2.42	2.26	1.92	Fe(OEP)(SPh)	DMF	2.42	2.27	1.92
Fe(PPIXDME)(SPh)[c]	N-MeIm	2.42	2.26	1.92		THF	2.35	2.26	1.95
Fe(PPIXDME)-(S-Cys(Ac)NHMe)[c,e]	N-MeIm	2.37	2.24	1.94	Fe(TPP)(SPh)[f]	THF	2.34	2.25	1.96
						camphor	2.37	2.27	1.94
Fe(PPIXDME)(SCH_2Ph)[c]	N-MeIm	2.34	2.23	1.95		S-Fe-N			
Fe(PPIXDME)($SC_6H_4NO_2$)	py	2.44	2.28	1.90	Cytochrome c[i]		3.06	2.24	1.24
Fe(PPIXDME)(SPh)[c]	py	2.41	2.27	1.92					
Fe(PPIXDME)($SC_6H_4NO_2$)	n-$PrNH_2$	2.48	2.26	1.90		O⁻-Fe-N			
Fe(PPIXDME)-(S-Cys(Ac)NHMe)[c,e]	n-$PrNH_2$	2.40	2.23	1.93	Fe(PPIXDME)($OC_6H_4NO_2$)	N-MeIm[j]	2.61	2.21	1.84
					Fe(PPIXDME)(OEt)	N-MeIm	2.44	2.15	1.92
Fe(OEP)($SC_6H_4NO_2$)	N-MeIm	2.42	2.26	1.90		Py	2.44	2.14	1.92
Fe(OEP)(SPh)[b]	N-MeIm	2.40	2.26	1.92	Fe(OEP)(OMe)	N-MeIm	2.43	2.15	1.92
Fe(OEP)($SC_6H_4NO_2$)	py	2.43	2.29	1.90					
Fe(OEP)(SPh)	py	2.40	2.28	1.92		N-Fe-N			
Fe(OEP)(SPh)	MeCN	2.41	2.29	1.91	[Fe(PPIXDME)-(N-MeIm)$_2$]$^+$[e]		2.90	2.29	1.57
Fe(TPP)(SPh)[f]	N-MeIm	2.39	2.26	1.93	[Fe(OEP)(N-MeIm)$_2$]$^+$		2.96	2.25	1.53
	$MeNH_2$	2.38	2.22	1.96	Cytochrome b_2[k]		2.99	2.28	1.49
	S⁻-Fe-S				Cytochrome b_5[l]		2.95	2.26	1.47
Fe(PPIXDME)($SC_6H_4NO_2$)	THT[g]	2.40	2.28	1.92					
Fe(PPIXDME)-(S-Cys(Ac)NHMe)[c,e]	THT	2.35	2.24	1.94	Fe(PPIX)Cl + $PhCH_2SH$[m]	BenzIm[n] (DMF[d])	2.40	2.26	1.93
Fe(PPIXDME)(SCH_2Ph)[c]	THT	2.31	2.23	1.96					
Fe(PPIXDME)($SC_6H_4NO_2$)	PhSH[h]	2.43	2.28	1.92	Fe(PPIX)Cl + PhCO-Cys-OMe[m]	BenzIm (DMF[d])	2.42	2.27	1.92
Fe(OEP)(SPh)	THT	2.38	2.27	1.93					
Fe(OEP)(SCH_2Ph)[c]	THT	2.32	2.23	1.95	FerriMb + MeSH[o]		2.46	2.24	1.94
Fe(TPP)(SPh)[f]	PhSH	2.40	2.25	1.97	FerriMb + n-PrSH[r] (pH 7.4)		2.39	2.24	1.94
					FerriHb + RSH (high pH)[p]		2.41	2.25	1.93
	S⁻-Fe-O								
Fe(PPIXDME)($SC_6H_4NO_2$)	DMF[e]	2.46	2.28	1.90	ox-P-450$_{cam}$[q]		2.45	2.26	1.91
Fe(PPIXDME)-(S-Cys(Ac)NHMe)[c]	DMF[e]	2.37	2.24	1.95	Microsomal ox-P-450[t]		2.41	2.25	1.91
					Mitochondrial ox-P-450[s]		2.42	2.26	1.91

[a] Isolated complex unless otherwise noted. [b] Measured in this work at ~95 K in toluene glass unless otherwise noted. [c] Generated in solution (see text). [d] Solvent. [e] DMF–CH_2Cl_2 (3:1 v/v) solvent. [f] Reference 26. [g] Tetrahydrothiophene. [h] Large excess gave only partial conversion to low-spin form. [i] I. Salmeen and G. Palmer, *J. Chem. Phys.*, 48, 2049 (1968). [j] [Fe(PPIXDME)(N-MeIm)$_2$]$^+$ also observed. [k] H. Watari, O. Groudinsky, and F. Labeyrie, *Biochim. Biophys. Acta*, 131, 592 (1967). [l] H. Schleyer, *Ann. N. Y. Acad. Sci.*, 212, 57 (1973). [m] Reference 23. [n] Benzimidazole. [o] Reference 22. [p] Reference 85. [q] Reference 51. [r] Reference 21. [s] Reference 84. [t] Y. Miyake, K. Mori, and T. Yamano, *Arch. Biochem. Biophys.*, 133, 318 (1969).

Results useful for examining the absorption spectral consequences of different types of axial ligation in low-spin complexes are unfortunately rather limited. Of the six low-spin spectra reported in Table XII, only three correspond to possible axial ligation in ox-P-450. Insufficient difference exists between the N-MeIm/N-MeIm and $SC_6H_4NO_2$/DMF cases, representing His/His and Cys-S/Asn(Gln) biological coordination, respectively, to permit secure ligation criteria to be established. However, EPR results in the following section for synthetic complexes and *b*-type cytochromes eliminate bis(imidazole) axial ligation. Recent spectral data[82] for metMb with 2-mercaptoethanol and cysteine methyl ester reveal Soret bands at 423–424 nm, and β and α bands at 545–548 and 572–582 nm, respectively. Spectra of the three thiolate PPIXDME base adducts and ox-P-450 cytochromes from different sources (Table XII) are in quite good agreement. Given the differences in temperature and solvent in the comparison and the inability to survey a range of Fe(PPIXDME)LL′ species, including those without sulfur ligands, we remark that the spectral similarities are consistent with, but do not require, thiolate coordination in the resting enzyme state.

(b) EPR Spectra. The spectra of the ox-P-450 state in all bacterial,[51,63] microsomal,[20,21,59b,62,63,83] and mitochondrial[84] enzymes are of the rhombic low-spin type[57,85] with g values at or near 2.4, 2.2, and 1.9. Some typical values are collected at the end of Table XIII. These values are widely recognized to be unusual for low-spin ferriheme proteins and, together with the 450-nm band of red-P-450·CO, have been principally responsible for numerous suggestions that at least one of the axial ligands is of a type not encountered in other cases. Speculation has centered on a sulfur ligand inasmuch as the EPR spectra afforded by the addition of thiols to oxidized Mb and Hb[3,21,22,85,86] and synthetic porphyrins[23,25,26,85b,86,87] (usually in the presence of a nitrogenous base) are unquestionably similar to those of ox-P-450. Recent EPR work utilizing an electric field effect[88] also points toward sulfur coordination in the enzymes. In all but the most recent experiments with synthetic porphyrins,[25,26] the initial species employed did not contain a bound sulfur ligand, and all EPR-detectable low-spin complexes were generated by addition of thiol, in some cases under conditions of unspecified acidity. Thiol addition to Mb or Hb is also reported to give two sets of EPR signals.[22] In several instances involving both proteins and synthetic complexes, it is not clear whether the low-spin EPR-active species were interpreted in terms of thiol or thiolate coordination. To provide a more certain definition of the relationship between g values and types of axial ligation in Fe(P)LL′ complexes, the two methods described above have been employed to generate low-spin species with a more diverse set of axial ligands than available heretofore. The results are given in Table XIII, whose organization follows that of Table V. Some representative spectra contrasting different ligation modes are shown in Figure 16. Six general types of axial ligation modes were accessible either by experimenta-

tion or utilization of EPR data for cytochrome *b* and *g* values are examined here in terms of their utility as empirical diagnostic indicators of axial coordination, an approach elaborated in crystal field terms by Peisach and Blumberg and embodied in their "truth" diagrams for low-spin ferrihemes.[85,87]

(i) **S^--Fe-N Ligation.** Addition of neutral N-bases to Fe(P)(SAr) in toluene solution causes diminution and eventual elimination of the high-spin signals (Figure 8) with concomitant appearance of a low-spin rhombic spectrum (Figure 16) assigned to Fe(P)(SAr)(N-base). When the base is of the imidazole type the spectra are clearly not those of $[Fe(P)(N\text{-base})_2]^+$, as the data in Table XIII and elsewhere[87] prove. Cleavage of $[Fe(P)]_2O$ with thiols in toluene yields compounds exhibiting high-spin EPR spectra. Addition of, or cleavage in the presence of, a coordinating base yields the same spectra, which for the appropriate case is the same as that obtained from isolated Fe(P)(SAr) + N-base. The *g* values show no important dependence on either the porphyrin or N-base, but the two aliphatic thiolate ligands tested produce a somewhat smaller *g*-tensor anisotropy than do arylthiolates with the same N-base. This behavior consistently occurs even when the sixth ligand is other than an N-base. *g* values of Fe(P)(SAr)(N-base) complexes are in very good agreement with those for the ox-P-450 state, and tend to favor Im over RNH_2 coordination in combination with an axial thiolate, i.e., favoring Cys-S-Fe-His over Cys-S-Fe-Lys(Arg) in the cytochromes. The close agreement between the results obtained using hemin chloride, Mb, Hb, and thiols (Table XIII) and those obtained in this work indicate that the species produced in the former case possess thiolate/N-base axial coordination. The same comment applies to the results obtained by Peisach et al.[87] in the TPP series.

(ii) **S^--Fe-S Ligation.** This mode involves coordination by thiolate and a neutral sulfur donor (thiol, thioether). Our attention was drawn to the possibility of thiol binding by the isolation of Fe(TPP)(SPh)(PhSH)[26] and the occurrence of six Cys residues in two P-450 cytochromes.[18] The EPR results discount neither of the possibilities Cys-S-Fe-L′, L′ = Cys-SH, Met.

(iii) **S^--Fe-O Ligation.** Coordination of neutral oxygen donors in the presence of bound thiolate affords spectra whose *g* values are similar to those exhibited by the preceding two ligation modes. Consequently, Cys-Fe-Asn(Gln) coordination, where DMF is used as a simulator of amide oxygen in Asn and Gln, cannot be eliminated in the cytochromes.

Of the three remaining categories of axial ligation examined, S-Fe-N, O^--Fe-N, and N-Fe-N, no complex or cytochrome representing these interactions exhibits either *g* values or *g*-tensor anisotropy close to those of the ox-P-450 state. The closest resemblance is found with Fe(PPIXDME)(OEt)L′, L′ = N-MeIm, py (Figure 16), whose middle *g* value is ca. 0.1 lower than that of ox-P-450. Deprotonation of a Ser or Thr side chain and stability of an acid-sensitive O^--Fe(III) bond under physiological conditions is improbable and without precedent; this type of ligation is rejected. At alkaline pH the bound Met residue of ferricytochrome *c* is reported to be displaced with probable formation of Lys-Fe-His axial coordination for which $g = \sim 3.4$, 2.07, 1.54.[89] If this interpretation is correct, the *g* values tend to eliminate this ligation mode in ox-P-450.

Certain axial ligation modes of the types O^--Fe-N,S,O based on L = ArO^-, RO^-, and OAc^- and L′ = RNH_2, THT, and DMF could not be examined owing to the lack of EPR-detectable low-spin species (Table V). This behavior emphasizes a significant difference between thiolate and anionic oxygen ligands. With all bases examined except water and ethanol, thiolate complexes form six-coordinate monoadducts. The amount of added base required for complete low-spin adduct formation, monitored by EPR, decreases in the order ArSH ≫ THF, DMF > THT > MeCN > py > N-MeIm. Fe(P)(OR) and Fe(P)(OAr) complexes form monoadducts only with the stronger bases py and N-MeIm; the diadduct $[Fe(PPIXDME)(N\text{-MeIm})_2]^+$ was also detected in the reaction of the *p*-nitrophenolate complex with excess N-MeIm. This base and Fe(PPIXDME)(OAc) under similar conditions yield only the diadduct. The tendency of thiolate complexes to form low-spin species with very weak ligands at low temperature is ascribed to a larger ligand field strength of ArS^- compared with the oxygen ligands, an effect observed with five-coordinate Fe(III) complexes of other tetraaza macrocycles.[24]

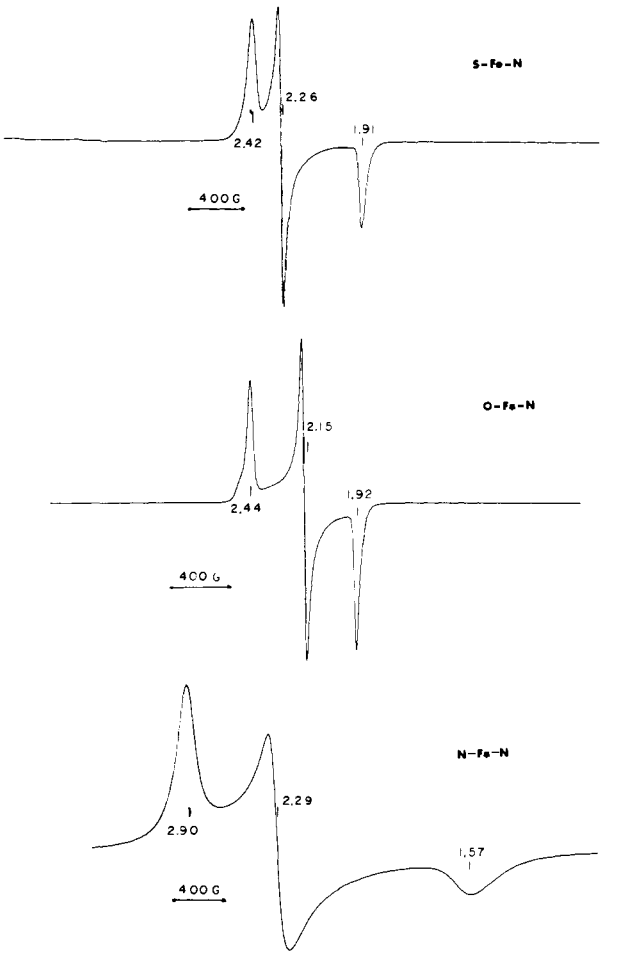

Figure 16. EPR spectra at ~95 K of $Fe(PPIXDME)(SC_6H_4NO_2)$(N-MeIm) in toluene glass, S-Fe-N; $Fe(PPIXDME)(OC_6H_4NO_2)$(N-MeIm) in toluene glass, O-Fe-N; $[Fe(PPIXDME)(N\text{-MeIm})_2]Cl$ in DMF-CH_2Cl_2 glass (3:1 v/v), N-Fe-N.

Synthetic Porphyrins as Ligation Models. The five- and six-coordinate porphyrin complexes studied here are intended only as the simplest models for certain types of axial ligation modes possible in principle for the oxidized P-450 reaction states. As such they suffer from obvious limitations, chief among which are their structurally unconstrained nature and the necessity to examine them outside even the most primitive protein environment. It is possible that the structure in and around heme iron in the oxidized enzymes departs significantly from that of synthetic species such as $Fe(PPIXDME)(SC_6H_4NO_2)$, but this point cannot as yet be assessed.[90] The tendency of alkylthiolate ligands, including Ac-Cys-NHMe, to provide a set of low-spin *g* values

less faithful to those of ox-P-450 than given by arylthiolates (Table XIII) may be viewed as a somewhat disconcerting inadequacy of the model approach. Alternatively, however, the intrinsically less basic arylthiolates may in fact better simulate (by EPR criteria) any Cys-S-Fe axial interaction present in the cytochromes. This proposal requires some modification of this interaction from that in unconstrained complexes by virtue of protein structural and environmental effects, leading to the possibility of an entatic condition[94] in and around the heme group. Earlier work[23] has shown that low-spin g values in Fe(PPIX)(SR)L′ complexes are moderately sensitive to thiolate basicity. Examination of comparative properties of other heme proteins and synthetic porphyrin complexes is beyond the purview of this report. Here we simply observe that both the absorption and EPR spectral parameters of two b-type cytochromes are in very good agreement with those of $[Fe(PPIXDME)(N\text{-}MeIm)_2]^+$, indicating that, at least in this case, a synthetic complex adequately conveys essential electronic features of biological hemes in fixed oxidation state with corresponding axial ligation.[81]

Summary and Conclusions. Noting carefully the modes of axial ligation which could not be directly tested (Table V) and with the expressed limitations of synthetic porphyrins as models for biological heme coordination, the following principal conclusions are drawn. (i) On the basis of collective comparative results from electronic absorption, MCD,[55] EPR, and Mössbauer spectra, the most probable axial ligation mode is Cys-S-Fe in the high-spin ox-P-450·S state, whose prosthetic group *primary* coordination stereochemistry is similar to that of $Fe(PPIXDME)(SC_6H_4NO_2)$. (ii) From comparative EPR and, marginally, electronic absorption spectra, the Cys-S-Fe coordination in ox-P-450-S is retained in the ox-P-450 state with axial ligation Cys-S-Fe-L′; no choice can be made among the possibilities L′ = His, Lys(Arg), Cys-SH, Met, and Asn(Gln), all of which have been tested. Conclusion ii is in substantial agreement with earlier EPR results cited above, many of which have been usefully quantified in "truth" diagrams by Peisach and Blumberg,[59b,85,87] who initially demonstrated the sensitivity of low-spin g values to variations in axial ligation. The methods employed in this work, as previously stressed, allow secure identification of axial ligands in all cases and tend to confirm the identity of these ligands, implicit or explicitly stated, in certain earlier investigations. This conclusion is somewhat more qualified with regard to the nature of L′ than that advanced previously on the basis of less information.[25] Our results, however suggestive, do not permit narrowing of the L′ possibilities above, but it is perhaps useful to observe that all characterized low-spin ferriheme proteins contain one or two coordinated Im(His) groups.

From conclusions i and ii the indicated simplified version of substrate binding follows, and is in agreement with explicitly represented earlier views[3,59b,86] concerning one or both reaction states except that a weakly bound sixth ligand is not included in the high-spin reaction state. Retention of thiolate coordination and removal of L′ upon substrate binding is at variance with an earlier view of sulfur ligand displacement,[51] but in accord with the proposal by Estabrook et al.[7b] that L′ = Im(His) is displaced. In another proposal[95] L′ = H_2O in ox-P-450, and this ligand is displaced when substrate is bound. We have been unable to detect H_2O binding to Fe(P)(SAr) by EPR measurements. To the extent to which 2-MeTHF may be considered a simulator of axial H_2O binding, spectral data for $Fe(PPIXDME)(SC_6H_4NO_2)$(2-MeTHF) (Figure 15, Table XII) widen the choice of L′ ligands to include H_2O. The intimate details of substrate binding and the attendant change in

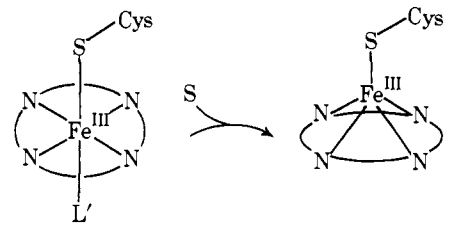

ox-P-450 (ls) ox-P-450·S (hs)

spin state, eq 2, are not known, but available results suggest that for $P\text{-}450_{cam}$ camphor binds in proximity to the heme.[35,96] It could be held by several types of interactions[76,35,96] including weak Fe···O coordination. However, this interaction cannot closely approach the strength of normal axial bond or else conversion to low-spin Fe(III) will occur, as has been observed for the system Fe(TPP)(SPh)/camphor in toluene at 77 K (Table XIII). In our hands under similar conditions a 100-fold excess of camphor with $Fe(PPIXDME)(SC_6H_4NO_2)$ and Fe(OEP)(SPh) failed to yield EPR-detectable low-spin species.

In assessing the ligation modes proposed above, due note is taken of the resemblance between certain electronic features of the oxidized P-450 reaction states and chloroperoxidase,[98] whose two cysteinyl residues are reported to exist as a disulfide in both the oxidized and reduced forms of the enzyme and thus are unavailable as thiolate ligands to iron.[98c] These results suggest that, at least in one case thiolate coordination may be a sufficient but not necessary condition for development of properties similar to those of oxidized P-450 reaction states. This situation is not consistent with the collective body of data for model PPIXDME complexes presented here.[103]

Finally, the results obtained here do not pertain directly to the reduced cytochrome P-450 reaction states shown in the reaction sequence 1. The report by Stern and Peisach[99] that a spectrum of the red-P-450·CO type is observed in a Fe(PPIX)/thiol/CO system under basic conditions has been followed by the development of chemically well-defined systems whose absorption[43,100,101] and MCD[100b] spectra provide strong evidence for Cys-S-Fe-CO coordination in the red-P-450·CO state. Recent discussions of the relation of this ligation mode to the physiologically significant red-P-450 states[99-101] and the relation of these states to reduced chloroperoxidase[98c,102] are available elsewhere.

Acknowledgments. This research was supported at the Department of Chemistry, M.I.T., by National Science Foundation Grant GP-40089X, at the Department of Chemistry, Northwestern University, by NIH Grant HL-13157, and at the Francis Bitter National Magnet Laboratory by the National Science Foundation. We thank Professor M. S. Wrighton for assistance in obtaining low-temperature electronic spectra and Professor H. H. Inhoffen for a generous gift of octaethylporphyrin. J.A.I. thanks the Lawrence Berkeley Laboratories for their hospitality during the period when the final x-ray structure calculations were performed.

Supplementary Material Available: tabular listings of root-mean-square amplitudes of vibration (Table IV) and structure amplitudes (45 pages). Ordering information is given on any current masthead page.

References and Notes

(1) (a) Department of Chemistry, M.I.T.; (b) Francis Bitter National Magnet Laboratory, M.I.T.; (c) Department of Chemistry, Northwestern University; (d) Department of Chemistry, Stanford University, Stanford, Calif. 94305

(2) S. G. Sligar, P. G. Debrunner, J. D. Lipscomb, M. J. Namtvedt, and I. C.

Gunsalus, *Proc. Natl. Acad. Sci. U.S.A.*, **71**, 3906 (1974). The more familiar P-450 usage will be retained in this paper.
(3) H. A. O. Hill, A. Röder, and R. J. P. Williams, *Struct. Bonding (Berlin)*, **8**, 123 (1970).
(4) (a) I. C. Gunsalus and J. D. Lipscomb, "The Molecular Basis of Electron Transport", J. Schultz and B. F. Cameron, Ed., Academic Press, New York, N.Y., 1972, pp 179–196; (b) R. W. Estabrook, J. Baron, M. Franklin, I. Mason, M. Waterman, and J. Peterson, *ibid.*, pp 197–230.
(5) V. Ullrich, *Angew. Chem., Int. Ed. Engl.*, 11, 701 (1972).
(6) R. Lemberg and J. Barrett, "Cytochromes", Academic Press, London, 1973, pp 73–96.
(7) (a) I. C. Gunsalus, J. D. Lipscomb, V. Marshall, H. Frauenfelder, E. Greenbaum, and E. Münck, *Biochem. Soc. Symp.*, **No. 34**, 135 (1973); (b) R. W. Estabrook, J. Baron, J. Peterson, and Y. Ishimura, *ibid.*, **No. 34**, 159 (1973).
(8) I. C. Gunsalus, J. R. Meeks, J. D. Lipscomb, P. Debrunner, and E. Münck, "Molecular Mechanisms of Oxygen Activation", O. Hayaishi, Ed., Academic Press, New York, N.Y., 1973, Chapter 14.
(9) J. E. Tomaszewski, D. M. Jerina, and J. W. Daly, *Annu. Rep. Med. Chem.*, **9**, 290 (1974).
(10) K. Dus, M. Katagiri, C.-A. Yu, D. L. Erbes, and I. C. Gunsalus, *Biochem. Biophys. Res. Commun.*, **40**, 1423 (1970).
(11) C. A. Tyson, J. D. Lipscomb, and I. C. Gunsalus, *J. Biol. Chem.*, **247**, 5777 (1972).
(12) C.-A. Yu, I. C. Gunsalus, M. Katagiri, K. Suhara, and S. Takemori, *J. Biol. Chem.*, **249**, 94 (1974).
(13) (a) Y. Imai and R. Sato, *Biochem. Biophys. Res. Commun.*, **60**, 8 (1974); (b) T. A. van der Hoeven and M. J. Coon, *J. Biol. Chem.*, **249**, 6302 (1974); (c) D. A. Haugen, T. A. van der Hoeven, and M. J. Coon, *ibid.*, **250**, 3567 (1975).
(14) F. P. Guengerich, D. P. Ballou, and M. J. Coon, *J. Biol. Chem.*, **250**, 7405 (1975).
(15) Abbreviations used in this paper: P-450$_{cam}$, camphor monooxygenase enzyme; P-450$_{LM}$, liver microsomal enzyme; P-450, cytochrome monooxygenases (general); PPIX, protoporphyrin IX dianion; PPIXDME, protoporphyrin IX dimethyl ester dianion; OEP, octaethylporphyrin dianion; TPP, tetraphenylporphyrin dianion; P, porphyrin dianion (general); Im, imidazole, imidazolyl; Cys-S, cysteinate (to emphasize thiolate sulfur coordination); Mb, myoglobin; Hb, hemoglobin.
(16) C.-A. Yu and I. C. Gunsalus, *J. Biol. Chem.*, **249**, 107 (1974).
(17) M. D. Maines and M. W. Anders, *Arch. Biochem. Biophys.*, **159**, 201 (1973).
(18) (a) R. L. Tsai, I. C. Gunsalus, and K. Dus, *Biochem. Biophys. Res. Commun.*, **45**, 1300 (1971); (b) K. Dus, W. J. Litchfield, A. G. Miguel, I. A. van der Hoeven, D. A. Haugen, W. L. Dean, and M. J. Coon, *Ibid.*, **60**, 15 (1974).
(19) B. L. Vallee and W. E. C. Wacker, "The Proteins," Vol. V, 2nd ed, H. Neurath, Ed., Academic Press, New York, N.Y., 1973, Chapter III.
(20) (a) H. S. Mason, J. C. North, and M. Vanneste, *Fed. Proc., Fed. Am. Soc. Exp. Biol.*, **24**, 1172 (1965); (b) K. Murikami and H. S. Mason, *J. Biol. Chem.*, **242**, 1102 (1967).
(21) C. R. E. Jefcoate and J. L. Gaylor, *Biochemistry*, **6**, 3464 (1969).
(22) E. Bayer, H. A. O. Hill, A. Röder, and R. J. P. Williams, *Chem. Commun.*, 109 (1969).
(23) A. Röder and E. Bayer, *Eur. J. Biochem.*, 11, 89 (1969).
(24) (a) S. Koch, S. C. Tang, R. H. Holm, and R. B. Frankel, *J. Am. Chem. Soc.*, **97**, 914 (1975); (b) S. Koch, R. H. Holm, and R. B. Frankel, *ibid.*, **97**, 6714 (1975).
(25) S. Koch, S. C. Tang, R. H. Holm, R. B. Frankel, and J. A. Ibers, *J. Am. Chem. Soc.*, **97**, 916 (1975).
(26) J. P. Collman, T. N. Sorrell, and B. M. Hoffman, *J. Am. Chem. Soc.*, **97**, 913 (1975).
(27) W. S. Caughey, "Inorganic Biochemistry", Vol. 2, G. Eichhorn, Ed., Elsevier, Amsterdam, 1973, Chapter 24.
(28) H. Ogoshi, H. Sugimoto, and Z. Yoshida, *Tetrahedron Lett.*, 2289 (1975).
(29) J. O. Alben, W. H. Fuchsman, C. A. Beaudreau, and W. S. Caughey, *Biochemistry*, **7**, 624 (1968).
(30) (a) N. Sadasivan, H. I. Eberspaecher, W. H. Fuchsman, and W. S. Caughey, *Biochemistry*, **8**, 534 (1969); (b) T. H. Moss, H. R. Lillienthal, C. Moleski, G. A. Smythe, M. C. McDaniel, and W. S. Caughey, *J. Chem. Soc., Chem. Commun.*, 263 (1972).
(31) H. H. Inhoffen, J. H. Fuhrhop, H. Voight, and H. Brockman, *Justus Liebigs Ann. Chem.*, **695**, 133 (1966).
(32) J. W. Buchler and H. H. Schneehage, *Z. Naturforsch., B*, **28**, 433 (1973).
(33) B. A. Averill, T. Herskovitz, R. H. Holm, and J. A. Ibers, *J. Am. Chem. Soc.*, **95**, 3523 (1973).
(34) See note at the end of this article concerning supplementary material available.
(35) (a) J. A. Peterson, *Arch. Biochem. Biophys.*, **144**, 678 (1971); (b) B. W. Griffin and J. A. Peterson, *Biochemistry*, 11, 4740 (1972).
(36) E. König, "Magnetic Properties of Coordination and Organometallic Transition Metal Compounds", Vol. 2, Landolt-Börnstein, New Series, Group II, Springer-Verlag, Berlin, 1966, pp 126–129.
(37) (a) J. L. Hoard, "Porphyrins and Metalloporphyrins", K. M. Smith, Ed., Elsevier, Amsterdam, 1975, Chapter 8; (b) J. L. Hoard, *Science*, **174**, 1295 (1971).
(38) High-spin Fe(III): (a) D. M. Koenig, *Acta Crystallogr.*, **18**, 663 (1965); (b) J. L. Hoard, M. J. Hamor, T. A. Hamor, and W. S. Caughey, *J. Am. Chem. Soc.*, **87**, 2312 (1965); (c) J. L. Hoard, G. H. Cohen, and M. D. Glick, *ibid.*, **89**, 1992 (1967); (d) A. B. Hoffman, D. M. Collins, V. W. Day, E. B. Fleischer, T. S. Srivastava, and J. L. Hoard, *ibid.*, **94**, 3620 (1972).
(39) Low-spin Fe(III): (a) D. M. Collins, R. Countryman, and J. L. Hoard, *J. Am. Chem. Soc.*, **94**, 2066 (1972); (b) A. Takenaka, Y. Sasada, E. Watanabe, H. Ogoshi, and Z. Yoshida, *Chem. Lett.*, 1235 (1972); (c) R. G. Little, K. R. Dymock, and J. A. Ibers, *J. Am. Chem. Soc.*, **97**, 4532 (1975).
(40) (a) E. Antonini and M. Brunori, "Hemoglobin and Myoglobin in their Reactions with Ligands" North-Holland Publishing Co., Amsterdam, 1971, Chapter 4; (b) M. W. Makinen, "Techniques and Topics in Bioinorganic Chemistry", C. A. McAuliffe, Ed., Macmillan Press Ltd., London, 1975, pp 21–59.
(41) (a) J. M. Rifkind, "Inorganic Biochemistry", Vol. 2, G. Eichhorn, Ed., Elsevier, Amsterdam, 1973, Chapter 25; (b) H. A. Harbury and R. H. L. Marks, *ibid.*, Chapter 26.
(42) D. Lexa, M. Momenteau, and J. Mispelter, *Biochim. Biophys. Acta*, **338**, 151 (1974).
(43) M. Millar and R. H. Holm, unpublished observations.
(44) L. Bullard, R. M. Panayappan, A. N. Thorpe, P. Hambright, and G. Ng, *Bioinorg. Chem.*, **3**, 161 (1974).
(45) (a) M. R. Snow and J. A. Ibers, *Inorg. Chem.*, **12**, 249 (1973); (b) J. J. Mayerle, S. E. Denmark, B. V. DePamphilis, J. A. Ibers, and R. H. Holm, *J. Am. Chem. Soc.*, **97**, 1032 (1975); (c) R. W. Lane, J. A. Ibers, R. B. Frankel, and R. H. Holm, *Proc. Natl. Acad. Sci. U.S.A.*, **75**, 2868 (1975).
(46) G. D. Fallon and B. M. Gatehouse, *J. Chem. Soc., Dalton Trans.*, 1344 (1975).
(47) The existence of charge-transfer interaction between the potential π-acceptor group *p*-nitrophenyl and the porphyrin ring is difficult to establish from the structural data. It is observed, however, that unconstrained Fe-S-C(Ph) angles in $[Fe_2S_2(S\text{-}p\text{-tol})_4]^{2-}$ (111°[45b]) and $[Fe_4S_4(SPh)_4]^{2-}$ (106°[48]) are somewhat larger than the 100° value found in this complex. Charge-transfer complexes between nitroaromatics and high-spin iron(III) porphyrins have been detected.[49]
(48) L. Que, Jr., M. A. Bobrik, J. A. Ibers, and R. H. Holm, *J. Am. Chem. Soc.*, **96**, 4168 (1974).
(49) G. N. La Mar, J. D. Satterlee, and R. V. Snyder, *J. Am. Chem. Soc.*, **96**, 7137 (1974).
(50) R. G. Little and J. A. Ibers, *J. Am. Chem. Soc.*, **97**, 5363 (1975).
(51) R. Tsai, C. A. Yu, I. C. Gunsalus, J. Peisach, W. Blumberg, W. H. Orme-Johnson, and H. Beinert, *Proc. Natl. Acad. Sci. U.S.A.*, **66**, 1157 (1970).
(52) M. Sharrock, E. Münck, P. G. Debrunner, V. Marshall, J. D. Lipscomb, and I. C. Gunsalus, *Biochemistry*, **12**, 258 (1973).
(53) D. W. Smith and R. J. P. Williams, *Struct. Bonding (Berlin)*, **7**, 1 (1970).
(54) (a) Reference 40, Chapter 3; (b) F. Mitani and S. Horie, *J. Biochem. (Tokyo)*, **66**, 139 (1969).
(55) J. H. Dawson, R. H. Holm, J. R. Trudell, G. Barth, R. E. Linder, E. Bunnenberg, C. Djerassi, and S. C. Tang, *J. Am. Chem. Soc.*, submitted for publication.
(56) P. M. Dolinger, M. Kielczewski, J. R. Trudell, G. Barth, R. E. Lindner, E. Bunnenberg, and C. Djerassi, *Proc. Natl. Acad. Sci. U.S.A.*, **71**, 399 (1974); L. Vickery, A. Salmon, and K. Sauer, *Biochim. Biophys. Acta*, **386**, 87 (1975).
(57) M. Weissbluth, *Struct. Bonding (Berlin)*, **2**, 1 (1967).
(58) J. Peisach and W. E. Blumberg, "Probes of Structure and Function of Macromolecules and Enzymes", Vol. II, B. Chance, T. Yonetani, and A. S. Mildvan, Ed., Academic Press, New York, N.Y., 1971, pp 231–239.
(59) (a) W. E. Blumberg and J. Peisach, *Ann. N.Y. Acad. Sci.*, **222**, 539 (1973); (b) J. Peisach, J. O. Stern, and W. E. Blumberg, *Drug Metab. Dispos.*, 1, 45 (1973).
(60) J. Peisach, W. E. Blumberg, B. A. Wittenberg, and L. Kampa, *Proc. Natl. Acad. Sci. U.S.A.*, **63**, 934 (1969).
(61) M. Kotani and H. Watari, "Magnetic Resonance in Biological Research", C. Franconi, Ed., Gordon and Breach, New York, N.Y., 1971, pp 75–96.
(62) J. Peisach and W. E. Blumberg, *Proc. Natl. Acad. Sci. U.S.A.*, **67**, 172 (1970).
(63) J. Peisach, C. A. Appleby, and W. E. Blumberg, *Arch. Biochem. Biophys.*, **150**, 725 (1972).
(64) This statement apparently does not apply to Fe(TPP)(SPh) for which *g* values of 8.6 and 3.4 have been reported.[26] If assignments corresponding to those above are made, $E/D = 0.11$ or 33% rhombicity.
(65) R. G. Shulman and G. K. Wertheim, *Rev. Mod. Phys.*, **36**, 459 (1964).
(66) (a) G. Lang, *Q. Rev. Biophys.*, **3**, 1 (1970); (b) A. J. Bearden, T. H. Moss, W. S. Caughey, and C. A. Beaudreau, *Proc. Natl. Acad. Sci. U.S.A.*, **53**, 1246 (1965).
(67) T. H. Moss, A. J. Bearden, and W. S. Caughey, *J. Chem. Phys.*, **51**, 2624 (1969).
(68) C. Maricondi, D. K. Straub, and L. M. Epstein, *J. Am. Chem. Soc.*, **94**, 4157 (1972); M. A. Torrens, D. K. Straub, and L. M. Epstein, *ibid.*, **94**, 4162 (1972).
(69) M. Blume, *Phys. Rev. Lett.*, **18**, 305 (1967).
(70) R. R. Sharma and P. Moutsos, *Phys. Rev. B*, 11, 1840 (1975).
(71) G. M. Harris, *J. Chem. Phys.*, **48**, 2191 (1968).
(72) G. Lang, T. Akasura, and T. Yonetani, *Phys. Rev. Lett.*, **24**, 981 (1970).
(73) A. Abragam and M. H. L. Pryce, *Proc. Roy. Soc. London, Ser. A*, **205**, 135 (1951).
(74) C. E. Johnson, *Phys Lett.*, **21**, 491 (1966).
(75) M. H. L. Pryce, *Nature (London)*, **164**, 116 (1949); B. Bleaney, *Philos. Mag.*, **42**, 441 (1951).
(76) G. Lang and W. Marshall, *Proc. Phys. Soc., London*, **87**, 3 (1966).
(77) N. Nakano, J. Otsuka, and A. Tasaki, *Biochim. Biophys. Acta*, **236**, 222 (1971).
(78) The approximation used in calculating H_{hf} is more valid the larger the applied magnetic field. In fitting the experimental data in Figure 12, therefore, the higher field points carried more weight.
(79) R. E. Dickerson, T. Takano, D. Eisenberg, O. B. Kallai, L. Samson, A.

Cooper, and E. Margoliash, *J. Biol. Chem.*, **246**, 1511 (1971); R. E. Dickerson, *Ann. N.Y. Acad. Sci.*, **227**, 599 (1974) (horse heart, bonito cyt. *c*).
(80) F. R. Salemme, S. T. Freer, Ng. H. Xuong, R. A. Alden, and J. Kraut, *J. Biol. Chem.*, **248**, 3910 (1973) (*R. rubrum* cyt. c_2).
(81) F. S. Mathews, M. Levine, and P. Argos, *J. Mol. Biol.*, **64**, 449 (1972) (calf liver cyt. b_5).
(82) T. Shimizu, T. Nozawa, M. Hatano, Y. Imai, and R. Sato, *Biochemistry*, **14**, 4172 (1975).
(83) Y. Miyake, K. Mori, and T. Yamano, *Arch. Biochem. Biophys.*, **133**, 318 (1969).
(84) J. A. Whysner, J. Ramseyer, and B. W. Harding, *J. Biol. Chem.*, **245**, 5441 (1970); S. C. Cheng and B. W. Harding, *Ibid.*, **246**, 7263 (1973).
(85) (a) Reference 58, pp 215–229; (b) W. E. Blumberg and J. Peisach, *Adv. Chem. Ser.*, **No. 100**, 271 (1971).
(86) H. A. O. Hill, A. Roder, and R. J. P. Williams, *Naturwissenschaften*, **57**, 69 (1970).
(87) J. Peisach, W. E. Blumberg, and A. Adler, *Ann. N.Y. Acad. Sci.*, **206**, 310 (1973).
(88) J. Peisach and W. B. Mims, *Proc. Natl. Acad. Sci. U.S.A.*, **70**, 2979 (1973).
(89) W. E. Blumberg, J. Peisach, B. Hoffman, E. Stellwagen, E. Margoliash, L. Marchant, J. Tulloss, and B. Feinberg, *Fed. Proc., Fed. Am. Soc. Exp. Biol.*, **32**, 469 (1973); D. O. Lambeth, K. L. Campbell, R. Zand, and G. Palmer, *J. Biol. Chem.*, **248**, 8130 (1973).
(90) It should be emphasized that detailed structural comparison between active sites or prosthetic groups in metalloproteins and synthetic analogues proposed as their minimal models is in a very formative stage. Owing to the lack of protein structural data which compare in precision to those of usual heavy-atom complex structures, such comparisons are presently limited to 1-Fe[91] and 4-Fe[91,92] iron–sulfur proteins and their synthetic analogues.[33,45c,46] Biological and synthetic 4-Fe clusters have nearly congruent structures whereas the 1-Fe analogue[45c] is an unconstrained (symmetrized) version of the Fe-S_4 center in rubredoxin proteins. Comparisons between forms of Mb and Hb and synthetic porphyrins have been assembled[40b,93] and the available protein data, while not highly precise, suggest some structural differences.
(91) L. H. Jensen, *Annu. Rev. Biochem.*, **43**, 461 (1974).
(92) S. T. Freer, R. A. Alden, C. W. Carter, Jr., and J. Kraut, *J. Biol. Chem.*, **250**, 46 (1975).
(93) R. G. Little and J. A. Ibers, *J. Am. Chem. Soc.*, **96**, 4452 (1974).
(94) B. L. Vallee and R. J. P. Williams, *Proc. Natl. Acad. Sci. U.S.A.*, **59**, 498 (1968); R. J. P. Williams, *Inorg. Chim. Acta, Rev.* **5**, 137 (1971).
(95) J. A. Peterson and B. W. Griffin, *Drug Metab. Dispos.*, 1, 14 (1973); B. W. Griffin and J. A. Peterson, *J. Biol. Chem.*, **250**, 6445 (1975).
(96) B. W. Griffin, S. M. Smith, and J. A. Peterson, *Arch. Biochem. Biophys.*, **160**, 323 (1974).
(97) G. C. Brackett, P. L. Richards, and W. S. Caughey, *J. Chem. Phys.*, **54**, 4383 (1971).
(98) (a) P. F. Hollenberg and L. P. Hager, *J. Biol. Chem.*, **248**, 2630 (1973); (b) P. M. Champion, E. Münck, P. G. Debrunner, P. F. Hollenberg, and L. P. Hager, *Biochemistry*, **12**, 426 (1973); (c) R. Chiang, R. Makino, W. E. Sponer, and L. P. Hager, *Ibid.*, **14**, 4166 (1975).
(99) J. O. Stern and J. Peisach, *J. Biol. Chem.*, **249**, 7495 (1974).
(100) (a) J. P. Collman and T. N. Sorrell, *J. Am. Chem. Soc.*, **97**, 4133 (1975); (b) J. P. Collman, T. N. Sorrell, J. H. Dawson, J. R. Trudell, E. Bunnenberg, and C. Djerassi, *Proc. Natl. Acad. Sci U.S.A.*, in press.
(101) C. K. Chang and D. Dolphin, *J. Am. Chem. Soc.*, **97**, 5948 (1975).
(102) P. M. Champion, R. Chiang, E. Munck, P. Debrunner, and L. P. Hager, *Biochemistry*, **14**, 4159 (1975).
(103) NOTE ADDED IN PROOF: The MCD spectrum of high-spin chloroperoxidase is highly suggestive of axial cysteinate coordination, contrary to chemical results:[98c] J. H. Dawson, J. R. Trudell, G. Barth, R. E. Linder, E. Bunnenberg, C. Djerassi, R. Chiang, and L. P. Hager, *J. Am. Chem. Soc.*, submitted for publication.

The Crystal Structure of $Na_2Fe(CO)_4 \cdot 1.5(C_4H_8O_2)$. Distortion of the $[Fe(CO)_4]^{2-}$ Anion in the Solid State

Henry B. Chin and Robert Bau* [1]

Contribution from the Department of Chemistry, University of Southern California, Los Angeles, California 90007. *Received August 7, 1975*

Abstract: The structure of $Na_2Fe(CO)_4 \cdot 1.5$(dioxane) has been solved by single-crystal x-ray diffraction methods. The most notable feature of the structure is the fact that the $[Fe(CO)_4]^{2-}$ anion is significantly distorted from tetrahedral symmetry: one of the C–Fe–C angles is 129.7°. There are basically two types of interactions between Na^+ and $[Fe(CO)_4]^{2-}$ ions: short-range Na–O interactions occurring at a distance of 2.32 Å and long-range Na···C and Na···Fe interactions occurring at distances of 2.95 and 3.09 Å, respectively. Two Na^+ ions and two $[Fe(CO)_4]^{2-}$ ions come together to form a curious, loosely held "cluster" in which each Na^+ ion is associated with the C–Fe–C regions of the anions. This unanticipated interaction between Na^+ and the C–Fe–C portion of $[Fe(CO)_4]^{2-}$ is probably responsible for the distortion of the C–Fe–C angle. The geometry of the $Na^+ \cdots$C–Fe–C region in this compound reflects the structural changes that take place in the $[Fe(CO)_4]^{2-}$ anion when a sodium ion is brought into close proximity, and suggests that some type of angular distortion may be occurring when $[Fe(CO)_4]^{2-}$ ion-pairs with Na^+ in solution. Crystallographic details for $Na_2Fe(CO)_4 \cdot 1.5$(dioxane) are: space group $P4_2/m$ (tetragonal), $a = 10.690$ (5) Å, $c = 12.283$ (6) Å, and $Z = 4$. Final R factor is 6.1% for 1175 independent reflections.

The application of $Na_2Fe(CO)_4$ as a "transition metal analogue of the Grignard reagent" has been vigorously explored by Collman and his co-workers during the past few years.[2-4] Many of the early synthetic applications of the potassium salt of the $[Fe(CO)_4]^{2-}$ ion were reported by Takegami, Watanabe, and co-workers during the late 1960's,[5] but initial investigations of these reactions were often complicated by the questionable purity of the carbonyl compound. The recent development of a convenient synthesis of high-quality $Na_2Fe(CO)_4$[6] has made possible a more systematic investigation of the synthetic utility of the carbonyl compound and a study of the mechanism of the reaction of the compound with organic substrates.[2,7]

In the course of mechanistic studies on $[Fe(CO)_4]^{2-}$ salts and their derivatives, it was noticed that the rates of many reactions involving these compounds were markedly dependent on the coordinating ability of the solvent and often also on the nature of the counterion. These observations were interpreted to indicate that tight ion pairs were being formed in solution between the alkali metal cations and the iron carbonylate anions.[3]

Ion pairing between metal carbonylate anions and alkali metal cations has long been suspected to exist in certain solutions;[8] although early investigations of the infrared spectra of $[Co(CO)_4]^-$ and $[Fe(CO)_4]^{2-}$ in water indicated the exclusive presence of tetrahedral ions,[9] it soon became evident that the carbonyl stretching region of these anions is highly solvent dependent. Thus $NaCo(CO)_4$ in THF (tetrahydrofuran) shows three bands in the ν_{CO} region, while in water and DMF (*N,N*-dimethylformamide) solutions only a single band is observed.[8] This in addition to conductivity data[10] suggested that ion pairs were being formed to vary-